Optimization of active power curtailment in grids with high renewable energy source penetration

André Felipe Pereira Pedroso

Dissertation presented to the School of Technology and Management of Bragança to obtain the double degree in Industrial Engineering.

Work oriented by:

Prof. Dra. Ângela P. Ferreira

Prof. Dr. Géremi Gilson Dranka

Bragança

2023

Optimization of active power curtailment in grids with high renewable energy source penetration

André Felipe Pereira Pedroso

Dissertation presented to the School of Technology and Management of Bragança to obtain the double degree in Industrial Engineering.

Work oriented by:

Prof. Dra. Ângela P. Ferreira

Prof. Dr. Géremi Gilson Dranka

Bragança

2023

Dedication

I dedicate this work to my loving family, who have always supported and encouraged me to pursue my goals.

Acknowledgement

First, I would like to express my deepest gratitude to my supervisors, Prof. Ângela Ferreira and Prof. Géremi Gilson Dranka, for their guidance and patience throughout the development of this work.

I would also like to thank Prof. Ana Pereira for providing valuable insights into the implementation of the algorithms used in this dissertation.

Finally, I thank the Polytechnic Institute of Bragança and the Federal University of Technology - Paraná for making this project possible and for providing me with this amazing experience.

Abstract

The high penetration of renewable energy in the distribution network can cause issues related to the imbalance between load and generation at certain moments, primarily due to the intermittent nature of these sources. This phenomenon has led to an increase in the curtailment of renewable energy and consequently in the regulation of this activity in order to limit these values.

In this scenario, the application of optimal power flow becomes relevant to ensure that energy dispatch is carried out efficiently and respecting the regulated and security limits of the electrical grid.

This study presents the application of a multi-objective optimization method to solve the optimal power flow problem in a transmission network with high penetration of renewable energy and the incorporation of a hydrogen-based energy storage system. The algorithm used aims to optimize the dispatch of renewable energy considering two objectives: reducing active system losses and reducing energy curtailment in wind and solar parks.

The results highlight the impact of the storage system in the curtailment of renewable energy and in the system losses, reducing both factors, and reinforcing the capability of these systems to improve network flexibility. Furthermore, the results demonstrate the efficiency of the multi-objective optimization method in representing and addressing both objective functions during the resolution of the proposed case study.

Keywords: Optimal power flow, Renewable energy curtailment, Hydrogen storage system

Resumo

A alta penetração de energia renovável na rede de distribuição pode causar problemas de desequilíbrio entre carga e geração de energia em certos momentos, principalmente devido à característica intermitente dessas fontes. Esse fenômeno resultou no aumento do corte da energia despachada por esses geradores e, consequentemente, na regulamentação dessa atividade para limitar esses valores.

Nesse cenário, a aplicação do fluxo ótimo de potência torna-se relevante para garantir que o despacho de energia seja realizado de maneira eficiente e respeitando as restrições regulamentadas e de segurança da rede elétrica.

Esse estudo apresenta a aplicação de um método de otimização multiobjectivo para solucionar o problema de fluxo potência ótimo em uma rede de transmissão com alta penetração de energia renovável e inclusão de um sistema de armazenamento de energia baseado em hidrogênio. O algoritimo utilizado tem como objetivo o despacho ótimo da energia renovavel considerando dois objetivos, a redução de perdas ativas do sistema e redução dos cortes de energia nos parques eólicos e solares.

Os resultados encontrados destacam o impacto do sistema de armazenamento no corte de energia renovável e nas perdas do sistema, reduzindo ambos fatores, reforçando a capacidade desses sistemas em aumentar a flexibilidade da rede. Além disso, os resultados demostraram a eficiência do método de otimização multiobjetivo em representar e lidar ambas funções objetivas durante a solução do caso de estudo proposto.

Keywords: Fluxo de potência ótimo, Corte de energia renovavel, Sistema de armazenamento por hidrogênio

Contents

Acknowledgement vii

Abstract ix

Resumo xi

Acronyms xxi

List of Symbols xxii

1 Introduction 1

1.1 Objective . . . 2

1.2 Dissertation structure . . . 3

1.3 Relevant publications . . . 3

2 State of the Art 5

2.1 Renewable energy curtailment . . . 5

2.2 Hydrogen Storage System . . . 7

2.2.1 Hydrogen cleanness and security . . . 10

2.2.2 Hydrogen production . . . 11

2.2.3 Hydrogen storage system . . . 19

2.2.4 Hydrogen fuel cells . . . 20

2.2.5 Hydrogen storage system and power systems . . . 22

2.3 Summary . . . 24

3 Optimal Power Flow **25**

3.1 OPF formulation . . . 27

3.1.1 Equalities constraints . . . 27

3.1.2 Inequalities constraints . . . 28

3.1.3 Optimization methods . . . 29

3.1.4 Interior Point Method . . . 31

3.1.5 Active-set method . . . 32

3.2 Multi-objective optimization . . . 33

3.2.1 Methods for solving MOOP . . . 34

3.2.2 Goal attainment method . . . 36

3.3 Summary . . . 38

4 Case Study **41**

4.1 IEEE 14 bus example grid . . . 42

4.2 Load and Generation . . . 42

4.2.1 Profile of load and generation . . . 47

4.3 Hydrogen Storage System . . . 47

4.3.1 Electrolyzer . . . 48

4.3.2 Hydrogen storage tank . . . 50

4.3.3 Fuel Cell . . . 50

4.3.4 Hydrogen storage system operation . . . 51

4.4 Renewable energy curtailment specification . . . 53

4.5 Optimization problem formulation . . . 54

4.5.1 Objective functions . . . 54

4.5.2 Constraints description . . . 55

4.5.3 Multiobjetive optimization approach and Pareto front . . . 55

4.6 Summary . . . 57

5 Results and discussion **59**

5.1 Pareto front . . . 61

5.2 Multi-objective approach analysis 62
5.3 Energy storage system analysis 64
5.4 Multi-objective approach with energy storage analysis 67
5.5 Summary 70

6 Conclusion and Future Work **71**

List of Tables

4.1 Vestas V100 - 2.0 MW wind turbine [52] 45
4.2 Description of each bus in the power grid 48
4.3 Nel Hydrogen - M-serie MC500 hydrogen generation system [56] 49
4.4 Ballard ClearGen - Hydrogen Fuel cell generator [57] 51
4.5 Rated characteristic of HSS 52
4.6 Values of OPF inequality constraints. 56

5.1 Overview of simulation performed in each section of the Results chapter . . 60
5.2 comparison of the annual operation of cases without HSS 64
5.3 Comparison of the annual operation of cases with HSS 70

List of Figures

2.1 Top countries in implemented non-dispatchable energy generation and maximum daily renewable share of net electricity in 2022 [2]. 6

2.2 Hydrigen economy roadmap planned by the European commission [9]. . . . 8

2.3 Hydrogen production methods 12

2.4 Water electrolysis reaction 15

2.5 Alkaline water electrolyzer 16

2.6 Proton exchange membrane electrolyzer 17

2.7 Solid Oxide electrolyzer 18

2.8 Hydrogen production methods 21

2.9 PEM fuel cells 22

2.10 Hydrogen production methods 24

3.1 Flow graph of Newton algorithm applied in OPF 31

4.1 IEEE 14-bus network 42

4.2 Wind speed histogram compared to Weibull model (PD). (a) Spring (b) Summer (c) Autumn (d) Winter 46

4.3 Total Load and RES generation during the four representative days 47

4.4 Neo hydrogen's steel tank [56] 50

5.1 Flowchart of the procedure for conducting the annual analysis of grid operation 60

5.2 Pareto front example for each representative day, (a) Spring, (b) Summer, (c) Autumn and (d) Winter 61
5.3 Total annual energy curtailed at each RES generator 62
5.4 Total annual transmission loss 63
5.5 Total Active power curtailment per hour 63
5.6 Total annual energy flow through transmission lines 64
5.7 Total annual energy curtailment 65
5.8 Comparing the impact of the HSS in the system active losses 65
5.9 Stored hydrogen level per hour. 66
5.10 Energy curtailment per hour 66
5.11 Total annual energy flow through the transmission lines during the representative days 67
5.12 Power exchange with slack bus per hour 68
5.13 Total annual energy curtailment in RES generators 68
5.14 Total annual transmission losses 69
5.15 Total annual energy curtailment per hour 69

Acronyms

AFC Alkaline Fuel Cells.

AWE Alkaline Water Electrolyzer.

DC Direct Current.

HSS Hydrogen Storage Systems.

IPM Interior Point Method.

MCFC Molten Carbonate Fuel Cells.

MOOP Multi-objective Optimization Problem.

OPF Optimal Power Flow.

PEM Proton Exchange Membrane.

PEMFC Polymer Electrolyte Membrane Fuel Cells.

RES Renewable Energy Sources.

SOE Solid Oxide Electrolyzer.

SOFC Solid Oxide Fuel Cells.

SQP Sequential Quadratic Program.

Symbols

x	Variables
I	Electric current
V	Voltage
Y	Admittance
S	Apparent power
P	Active power
Q	Reactive power
θ	Voltage angle
δ	Admittance angle
$L(x)$	Lagrangian function
$H(x)$	Hessian function
J	Pareto front element
w	Objective function weight
P_{wind}	Wind turbine power
P_r	Generator rated power
v	Wind turbine velocity
v_r	Wind turbine rated velocity
v_c	Wind turbine cut-in velocity

v_r	Wind turbine cut-off velocity
f_w	Weibull probabilistic density function
P_{pv}	Photovoltaic power
S	Panel surface area
G	Irradiation
$M_{H_2}^{prod}$	Mass of Hydrogen produced
$M_{H_2}^{el}$	Mass of Hydrogen consumed
P_{ez}	Electrolizer power
P_{FC}	Fuel cell power
L_{H_2}	Level of hydrogen stored
E	Renewable energy curtailed
D	Energy curatailed standart deviation
P_{loss}	Grid transmission losses
C_{total}	Total energy curtailed

Chapter 1

Introduction

Environmental issues related to the emission of CO_2 have been a significant concern in recent decades, leading many countries to invest in the decarbonization of their energy sectors. This commitment has resulted in an increasing installation of renewable energy source generators in the electric grid, which can be considered the foundation of the current energy transition scenario. However, the intermittent nature of these generators can cause operational problems in the energy distribution system, such as line congestion, bus overvoltages, and changes in the rated frequency of the system.

To prevent interruptions in the normal operation of the electrical grid, network operators implement curtailments of renewable energy generation to ensure a balance between load and generation. However, these activities are regulated in many countries to prevent them from exceeding specified annual limits and to follow specific instructions. This has led to research efforts aimed at analyzing efficient methods for dealing with excess energy production.

One of the most promising methods for addressing this issue is the implementation of energy storage systems at strategic points in the grid to alleviate the impact of dispatched energy during periods of peak production and low consumption.

Today, many categories of energy storage systems are available on the market. Specifically in power system applications, pumped-hydro storage and batteries are the most

widely applied worldwide and are dealt extensively in literature. However, another technology is gathering attention due to its flexible operation, applicability, and environmental friendliness: hydrogen storage systems (HSS).

In this context, ensuring that the grid security limitations are being followed and making efficient decisions with regard to the energy dispatched by renewable generators and energy storage system operations are essential matters. For that reason, Optimal Power Flow (OPF) is usually applied to simulate grid behavior and determine optimal decisions, taking into account the objectives defined by the operator.

1.1 Objective

The main objective of this study is to present a multi-objective optimization method for solving the OPF problem in order to define the optimal dispatch of renewable energy and the operation of an HSS. The study also aims to evaluate the impact of the HSS on the energy curtailment of renewable source generators and on the transmission losses of the grid.

To achieve this goal, the work is divided into several key steps. First, the operation of the case study is analyzed by comparing a multi-objective optimization approach with the standard single-objective approach, taking into account the objective functions explained earlier. The primary focus here is to verify the functionality of the multi-objective approach.

In the next step, an energy storage device is integrated into the case study network, and the results of optimal grid operation before and after this integration are compared. This section specifically aims to evaluate the impact of energy storage on renewable energy curtailment and transmission losses.

Finally, a multi-objective optimization approach designed for operating with the HSS is tested. In this case, the goal is to evaluate the proposed method's effectiveness and determine if it can improve the overall grid operation.

1.2 Dissertation structure

This study is organized in the following chapters:

- Chapter 1 - Introduction: This chapter provides a brief context of the main topic of this dissertation, its objectives, and the structure of this work.
- Chapter 2 - State of the Art: This chapter offers a deeper explanation of the themes addressed in the dissertation. The chapter itself is divided into the two main concepts applied in this study: Renewable energy curtailment and Hydrogen storage system.
- Chapter 3 - This chapter aims to contextualize the OPF problem and present the methodology applied in this work for analyzing and solving a multi-objective optimization problem.
- Chapter 4 - Case of study: Here is presented case study in which the simulations of this work were carried out. The chapter explains the methodology used to build the models of the equipment added to the network, as well as the implementation of the optimization methods used.
- Chapter 5 - Results: In this chapter, the results obtained through the proposed methods are displayed, along with a detailed analysis of these data.
- Chapter 6 - This chapter presents the conclusions of this study and provides a final evaluation of the methods applied and the results obtained in this dissertation. Additionally, some suggestions for further analyses that could be conducted are proposed.

1.3 Relevant publications

During the implementation of this work, several conference papers have been published, namely

1. A. Pedroso, Y. Amoura, A. I. Pereira and Â. Ferreira, "A Hybrid Genetic Algorithm for Optimal Active Power Curtailment Considering Renewable Energy Generation," in *Computational Science and Its Applications – ICCSA 2023 Workshops*, O. Gervasi, B. Murgante, A. M. A. C. Rocha, *et al* Eds., Cham: Springer Nature Switzerland, 2023, pp. 479–494, DOI: 10.1007/978-3-031-37108-0_31

2. A. Pedroso, G. Zanatta, A. Ferreira, et al., "An improved ga-based approach for reduced non-discriminatory renewable energy curtailment," *International Conference on Electricity Distribution - CIRED 2023*, Jun. 2023, in press.

3. Y. Amoura, A. Pereira, J. Lima, A. Ferreira, A. Pedroso and S. Torres, "Multi-Objective Optimal Sizing of an AC/DC Grid-Connected Microgrid System", *International Conference on Optimization, Learning Algorithms and Applications - OL2A 2023*, Sep. 2023, in press

Chapter 2

State of the Art

In this chapter, the state of the art of the main topics addressed in this study is presented, including an overview of the history, technical aspects, and applications of each theme. The chapter is divided into two sections: Renewable Energy Curtailment and Hydrogen Storage Systems.

The section contextualizes the impacts of the energy sector's transactions worldwide, which is leading to an increasing dispatch of renewable energy in the most affected countries. It also proposes some strategies to mitigate these incidents.

The sections, on the Hydrogen Storage System provide an overview of the role of hydrogen in the current energy sector and its applications as an energy storage system.

2.1 Renewable energy curtailment

In this work, the term renewable energy curtailment refers to the choice made by the electric grid operator not to dispatch the entire energy available in a renewable source power plant. This decision affects investors in this sector and can be considered a waste of natural resources. Typically, the curtailment occurs due to the oversizing of the generation system and the limited capacity of the energy transmission lines [1].

The curtailment of renewable energy is closely related to the high penetration of Renewable Energy Sources (RES) in power systems. It can reach significant levels in

countries that have heavily invested in the energy transition shift for a more sustainable energy sector. For example, in California, USA, in 2020, approximately 1.4 TWh of renewable energy was curtailed, equivalent to roughly 5% of the total annual energy generated in the state. Similarly, in the United Kingdom during 2021, the annual curtailed renewable energy amounted to about 7 TWh, accounting for about 4% of total energy generation [2].

As mentioned previously, curtailment typically occurs due to the limited options available to dispatch the available energy. However, planning can become quite complex when dealing with RES generation, such as solar and wind power plants, which have seen significant growth in recent years and in some countries, as shown in Figure 2.1, can achieve high shares of the energy production during some periods. The nondispatchable nature of these technologies not only makes it challenging to efficiently plan the future yield of energy but can also effect the grid stability [3].

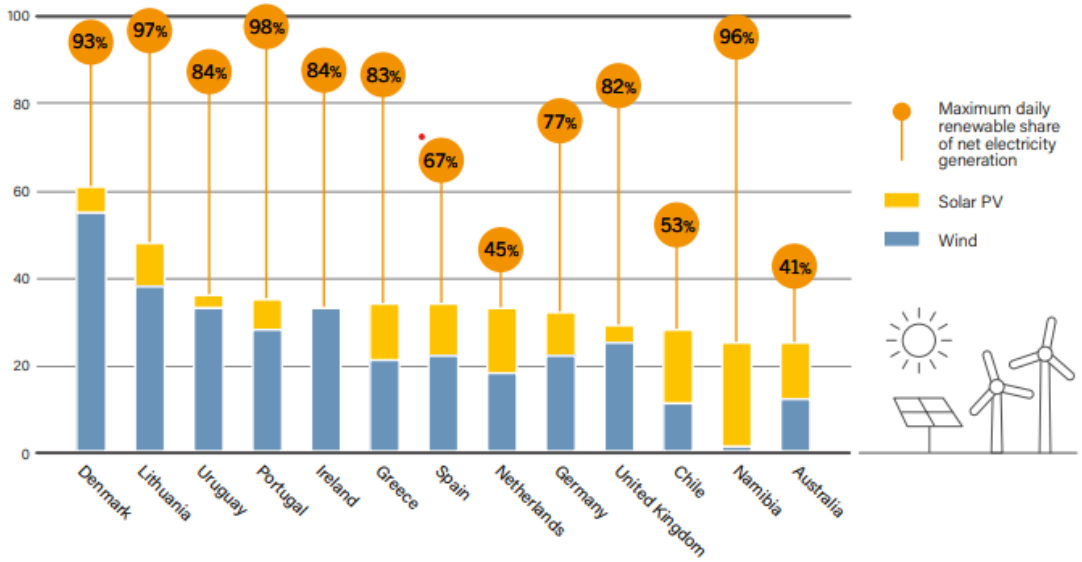

Figure 2.1: Top countries in implemented non-dispatchable energy generation and maximum daily renewable share of net electricity in 2022 [2].

Since maintaining the grid operation is crucial, energy curtailment is a practice that many countries adopt, for example, in [4] is presented an international review of some of the experiences with energy curtailment and the methods used to avoid it. To mitigate

the renewable energy curtailment, governments have imposed limits on the maximum annual allowable curtailed energy, and exceeding these limits can result in penalties for the operators. In the European Union, the Regulation (EU) 2019/943, on the internal market for electricity has established a curtailment limit of 5% of the energy generated by a RES power plant, although some countries may adopt lower values. Furthermore, the regulation established that the curtailment decisions should be non-discriminatory among all the generators connected to the grid [5].

To meet these standards, various techniques can be employed to improve the grid's capacity to manage excess generated energy and increase its flexibility. Some of the most common methods include the implementation of energy storage systems, which include a wide range of technologies, expansion of the transmission system, improvements in forecasting methods and inclusion of flexible loads through demand response programs [4].

Regarding the non-discriminatory nature of dispatching and curtailing renewable energy, different methods are applied worldwide, each with its own advantages. Therefore, there is no consensus on the correct approach to dealing with this problem. The techniques used to determine the order of energy dispatch are known as the Principle of Access, some examples of these methods are discussed in [5].

Regarding energy curtailment, approaches can also vary. In [6], the author applies penalty terms during energy dispatch planning to ensure a more equitable curtailment among RES generators connected to the grid. This issue is also addressed in [7], where distribution factors are included in the OPF formulation. These factors help mitigate total energy curtailment and promote non-discriminatory system operation.

2.2 Hydrogen Storage System

Although hydrogen technologies have found vast applications in the industrial sector and benefit from a concrete and extensive bibliography, their influence in the power sector has increased significantly only in recent decades. This growth can be largely attributed to

the motivation and investments made by the global initiative to promote low-carbon or CO_2-emission-free technologies. As a result, numerous policies are being implemented to encourage the production of green or blue hydrogen to meet the current market demands [8].

A recent example of this new scenario is the European Clean Hydrogen Alliance project, launched in July 2020 by the European Commission. The primary objective of this project is to regulate and promote projects involved in the efficient production, transmission, and distribution of hydrogen. Figure 1 shows a roadmap for hydrogen standardization proposed by the European Commission, focusing specifically on the expansion of green hydrogen production. However, it is important to note that the project also includes the production and application of other types of hydrogen without discrimination [9].

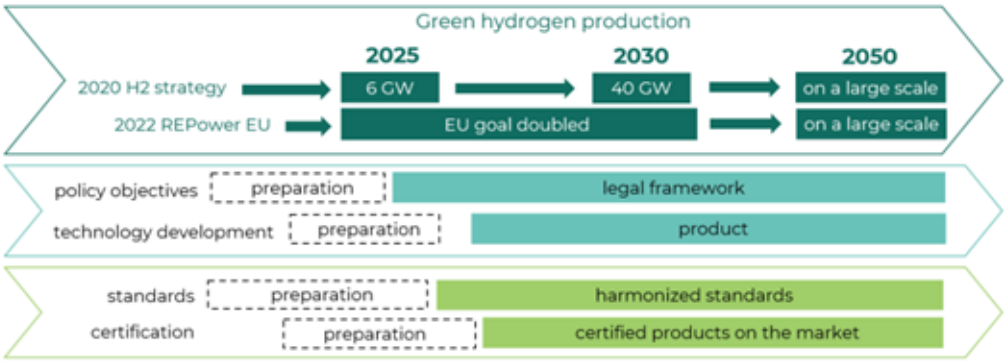

Figure 2.2: Hydrigen economy roadmap planned by the European commission [9].

Hydrogen is also being considered as an option for energy storage, which can help alleviate the high pressure of renewable energy on the electrical grid. Although the overall efficiency of producing green hydrogen is still far from competing with most conventional energy storage methods, this technology is attracting significant attention due to its high energy storage capacity, mobility, and versatility in various applications, such as vehicle fuels, heating, or electricity generation [10].

The belief that hydrogen is the future of the energy sector is not a recent trend; in fact, the term "hydrogen economy" was already employed back in 1976 at the first

World Hydrogen Conference. At that time, the high impact of the oil crisis created a favorable environment for the rise of an alternative substance that could replace the highly predominant oil-based economy. The process of producing hydrogen was already well known, and the main topic debated at the conference, proposed by John Bockris, was the possibility that distributing hydrogen using pipes could be more efficient than distributing energy using copper cables. The main conclusion drawn, after all, was that distributing hydrogen was indeed more efficient in transporting energy over long distances. However, when considering the overall process, the energy conversion and infrastructure costs, were significant drawbacks to this method [11] [12].

Although the idea of a hydrogen economy was appealing, during its initial years after the conference in which it was introduced, the field experienced slow growth in research, followed by stagnation. This phenomenon could be attributed to the low oil prices at that time. However, in the early 2000s, the sector regained the spotlight as the greenhouse effect became a relevant global concern and technologies capable of reducing CO_2 emissions were attracting significant attention. During that time, some models predicted a high penetration of hydrogen-driven technology in society by 2020 to 2030. Reports such as the HyNet Project [13] and the High-Level Group on Hydrogen and Fuel Cells [14] present fuel cell vehicles as the primary candidates for clean fuel vehicles in the future. Nevertheless, these estimations were not achieved [8].

One theory explaining why the hydrogen economy did not grow as much as predicted at the beginning of the millennium revolves around two principal points. First, there was the belief that hydrogen could lead to a carbon-free energy sector, which was unattainable due to the fact that a significant portion of hydrogen was and still is produced from natural gas and methane through chemical reactions that emit CO_2. Second, the focus on vehicle applications presented considerable drawbacks, as hydrogen production and storage were considerably more expensive than other options [11].

However, as mentioned before, since the growth of renewable energy production and also after COVID-19, interest in the hydrogen economy has been increasing once again. The current scenario of price reductions of electronic devices, excess electrical energy

during peak intermittent production, overloaded grids in countries with high penetration of renewable energy generation, and the implementation of low-carbon policies worldwide, when combined, could represent a turning point for the hydrogen economy, potentially establishing hydrogen as a crucial player in the energy sector.

The following sections focus on studying the application of hydrogen storage systems in power grid applications with the presence of RES production. Since the technology for storing hydrogen in connection with the grid also involves the application of electrolyzers and fuel cells, some of the main methods will also be addressed.

2.2.1 Hydrogen cleanness and security

Before we discuss technologies for hydrogen production, it is necessary to understand several essential factors related to the application and generation of hydrogen. These include the cleanliness of this energy vector in terms of its carbon footprint, as well as its safety when applied in everyday situations. These factors constitute an important aspect that could determine the future utilization of hydrogen within the energy sector.

Despite its optimistic potential as a future energy carrier, hydrogen's inflammable nature has led to associations with explosions and accidents. However, some individuals believe that hydrogen can be managed to pose an accident risk similar to that of other fuels commonly used on the market [15].

This factor is extremely important to create a trustworthy perspective for the users, especially in applications within the transportation sector. Accidents are more likely in this sector, given the inherent challenge of monitoring all environmental variables and potential scenarios.

Regarding the cleanliness of hydrogen, one of the main arguments supporting its role as a future energy carrier is its environmentally friendly nature. It does not emit greenhouse gases when used for energy generation, whether through combustion or fuel cells. However, as mentioned previously, hydrogen can be produced through a variety of reactions, many of which rely on fossil fuels and emit a quantity of carbon gases.

Therefore, it is crucial to establish the carbon footprint of the hydrogen used for each application. Otherwise, there is no point in investing in hydrogen as a clean method for energy storage and transportation while implementing technologies that rely on fossil fuels. To prevent this confusion, a color-standardization method has been developed to classify hydrogen on the basis of its production method. The categories include gray, blue, and green

Gray hydrogen is produced through technologies that rely on fossil fuels, including natural gas and coal. More recently, the development of blue hydrogen production methods has emerged, and in this case, fossil fuels are still used as feedstocks, but technologies are employed to capture the CO_2 emitted during the process. As a result, these methods are considerably more environmentally friendly compared to the previous methods. Lastly, there is green hydrogen, produced through carbon-free methods in which the energy supplied to the production plants is derived from renewable energy sources (RES) generators, which makes it completely sustainable [16].

Understanding the color standardization of hydrogen production technologies is crucial to proceeding with this chapter, given that the environmental cleanliness of hydrogen has become a significant factor over the past few decades and helped drive investments in green hydrogen research and its applications within the energy sector.

2.2.2 Hydrogen production

Hydrogen is an element that has been known for more than 200 years; the gas was first identified by Henry Cavendish in 1776 and later, in 1783, was named by Antonie Lavoisier. At the time it was already known that this gas was inflammable which resulted in the employment of hydrogen as a fuel for balloons, which were the first aircraft. Later the gas became very important since it was highly employed in the launch of space shuttles. At that time, the method for generating hydrogen was discovered by the reaction of dilute sulfuric acid on iron [15].

Since it was realized the importance of hydrogen as an energy carrier, it became relevant to developing methods for producing the gas as efficiently as possible. The first production of hydrogen on a marked-size scale happened around 1920, and the composition was made by electrolyzing water, one of the first methods invented. Later this process was replaced by methods that used fossil fuels as feedstock, which were cheaper than the previous method.

Today, fossil fuels are still the predominant method for supplying the world's demand for hydrogen, especially the use of natural gas [17]. However, there are a variety of process technologies that can be applied for this objective, including chemical, biological, electrolytic, photolytic, and thermochemical, each of which has its own benefits and challenges. Figure 2.3 presents some of the main method for hydrogen production, separating the fossil-fuels based and renewable sources based methods.

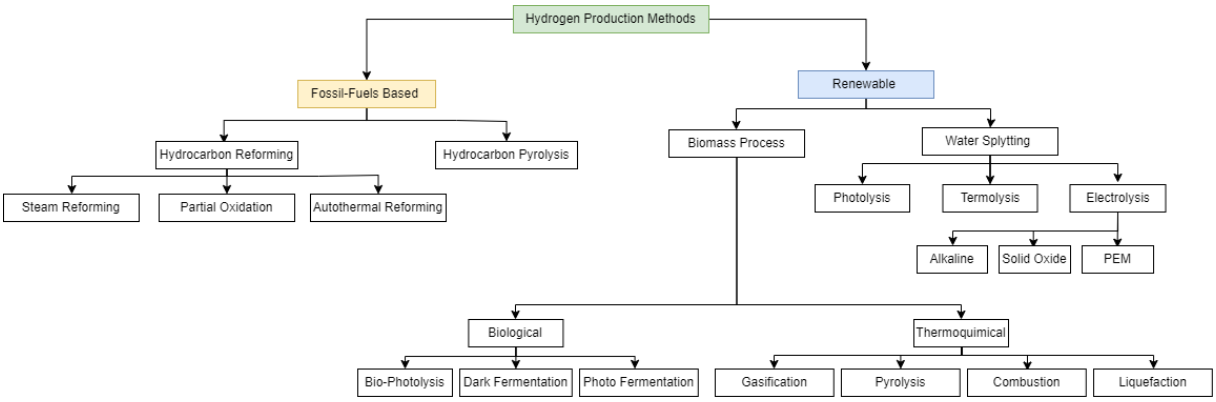

Figure 2.3: Hydrogen production methods

As a result, defining the most suitable hydrogen production method can be quite complex, since it depends on various factors such as feedstock availability, application, and even national policies. Thus, this section will provide an overview of the main technologies for hydrogen production and their respective characteristics.

Hydrogen produced by fossil fuels

Methods for generating hydrogen using fossil fuels primarily involve processes that extract hydrogen from hydrocarbons within the fossil fuels. Some of the main processes applied

today include steam reforming, partial oxidation, gasification, and others.

The Steam Reforming process stands as one of the main techniques for large-scale hydrogen production. It finds extensive use in the chemical and energy industries to derive hydrogen from hydrogen-rich molecules, such as natural gas, methanol, glycerol, and ethanol. This process essentially involves converting hydrocarbons and water vapor into carbon monoxide and hydrogen [18]. Natural gas is the most widely used feedstock and its conversion can be described as follows:

$$CH_4 + H_2O + \text{heat} \rightarrow CO + 3H_2 \tag{2.1}$$

After conversion, a second reaction known as the water-gas shift is typically applied to increase hydrogen production [19]. It can be described as follows:

$$CO + H_2O \rightarrow CO_2 + H_2 + \text{heat} \tag{2.2}$$

In the partial oxidation process, natural gas is burned with oxygen, resulting in carbon monoxide and hydrogen. This method is recognized for its high efficiency, usually around 70-80%. However, the elevated temperature caused by the exothermic nature of the reaction diminishes the cost-effectiveness of the system, particularly in large-scale plants [20]. The water-gas shift process can also be implemented in this context to improve the hydrogen yield. The partial oxidation process can be described as:

$$CH_4 + 0.5O_2 \rightarrow CO + 2H_2 + \text{heat} \tag{2.3}$$

Coal is also widely used for hydrogen production, because of its abundant supply that is accessible worldwide. The gasification process is used to produce hydrogen from coal. There are various variations of this method, such as fixed-bed or fluidized-bed gasification [18]. A typical coal gasification reaction can be described as follows:

$$C + H_2O + \text{heat} \rightarrow CO + H_2 \tag{2.4}$$

Carbon Capture Methods

Until now, all methods presented for hydrogen production fall under the category of gray hydrogen production, as they generate a substantial quantity of CO_2 as the final product. The problem is, when dealing with endothermic processes, such as steam reforming or gasification, achieving sustainability becomes quite a challenge, not only the produced CO_2 must be managed, but also the energy source utilized to generate the reaction's heat must originate from a sustainable process.

Despite this challenge, several methods have been proposed to make fossil fuel-based hydrogen production more environmentally friendly. These processes involve the capture and storage of CO_2 produced during the process and are collectively known as decarbonization. The methods used for CO_2 capturing are usually divided into post-combustion, pre-combustion, and oxyfuel combustion. Some studies point out that these methods can reduce the emission of CO_2 up to 90% in steam-reforming hydrogen plants. At the end of this process, the hydrogen produced in the plant is considered blue hydrogen [19].

Hydrogen production based on renewable sources

To achieve carbon-free hydrogen production, referred as green hydrogen, it is necessary that all processes involved in hydrogen production, including the reagents and products, are sustainable and do not emit any greenhouse gases. Only a few processes meet these requirements, and one of the most typical and relevant is water electrolysis.

The process of water electrolysis has been well known for over 200 years, first documented by Jan Rudolph Deiman and Adriaan Paets van Troostwijk in 1789. This method essentially involves producing hydrogen by applying an electric field to dissociate water molecules into hydrogen (H_2) and oxygen (O_2) [21]. An illustration of this reaction is presented in Figure 2.4.

When the DC voltage source is connected to each of the metallic plates (electrodes), the current supplied by the source passes through the solution, causing the hydrogen ions to be drawn to the cathode where they are neutralized by the current, producing hydrogen

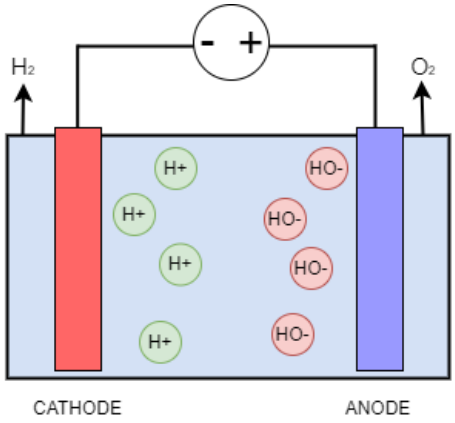

Figure 2.4: Water electrolysis reaction

gas. Simultaneously, the hydroxide ions are attracted to the anode, generating oxygen. The typical reactions that occur at the cathode and anode are described as follows [22],

$$2H^+ + 2e^- \rightarrow H_2 \tag{2.5}$$

$$4HO^- \rightarrow O_2 + 2H_2O + 4e^- \tag{2.6}$$

and the overall cell reaction,

$$2H_2O \rightarrow 2H_2 + O_2 \tag{2.7}$$

The operating principles of the electrolysis technologies that are predominantly used today are essentially the same. What varies in each process are the ionic agents (OH^-, H^+, O^2-) and certain operating conditions [23]. The primary methods for water electrolysis are (1) Alkaline Water Electrolyzer (AWE), (2) Solid Oxide Electrolyzer (SOE), and Proton Exchange Membrane (PEM) electrolyzer. "

Alkaline water electrolyzer: AWE has been the most applied sustainable method for hydrogen production and is a well-established technology. The particularities of this

method are the use of an alkaline solution as electrolyte liquid, and the diaphragm separator, membrane, used to separate both polarities of the cell. An illustration of AWE is present in Figure 2.5.

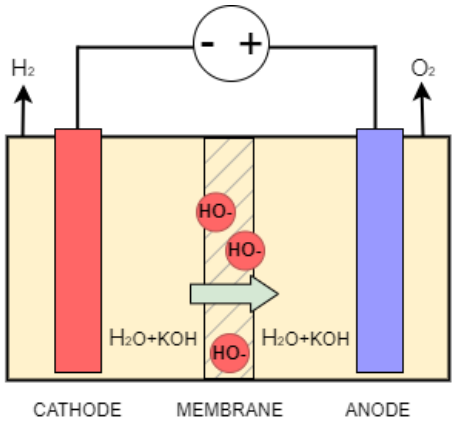

Figure 2.5: Alkaline water electrolyzer

In the anode polarity of the cell, the reaction that occurs is described as,

$$4OH^- \rightarrow O_2 + 2H_2O + 4e^- \tag{2.8}$$

and at the cathode polarity:

$$2H_2O + 2e^- \rightarrow H_2 + 2OH^- \tag{2.9}$$

A common electrolyte solution used in AWE is potassium hydroxide in a concentration of around 30%, operating at a temperature of 70°C-80°C. The substance's alkaline proprieties increase substantially the conductivity of the solution and the use of the membrane ensures the ionic contact between the electrodes and prevents the product gases from mixing. The drawbacks of this method are its low current density, which does not exceed 400 mA / cm^2, and its efficiency, which is around 60% [24].

Proton exchange membrane electrolyzer: One technology that is gaining popularity for renewable energy applications in hydrogen production is the PEM electrolyzer.

This method is distinguished by its higher current density, rapid response, and production of high-purity and high-pressure hydrogen, making it a compelling choice for use in the energy sector, such as in electrical vehicles. The principle of operation of this device is the separation of the cathode and the anode by a polymer electrolyte membrane, which allows the passage of hydrogen ions (protons) exclusively [23]. The figure below illustrates a PEM electrolyzer.

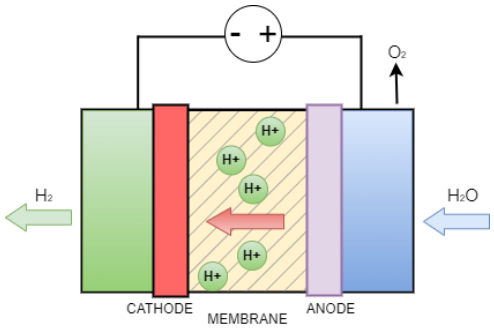

Figure 2.6: Proton exchange membrane electrolyzer

The operation begins with water being pumped to the anode, where it is dissociated into oxygen and protons. The protons migrate towards the negative polarity of the system and pass through the membrane to reach the cathode side. There, the protons combine with electrons to form hydrogen. The reactions occurring at the anode and cathode are described as follows:

$$2H_2O \rightarrow 4H^+ + O_2 + 4e^- \tag{2.10}$$

$$4H^+ + 4e^- \rightarrow 2H_2 \tag{2.11}$$

Solid Oxide electrolyzer: Different from the AWE and PEM technologies, SOE doesn't employ a liquid solution for the process of water electrolysis. Instead, it uses water steam. As a result, cells must operate at much higher temperatures compared to other methods, typically over 500 °C. In this case, the polarities are also separated by a membrane. However, in this scenario, a ceramic membrane is used, which allows only oxygen ions to pass

to the anode [25]. An illustration of an SOE cell is provided in the figure below,

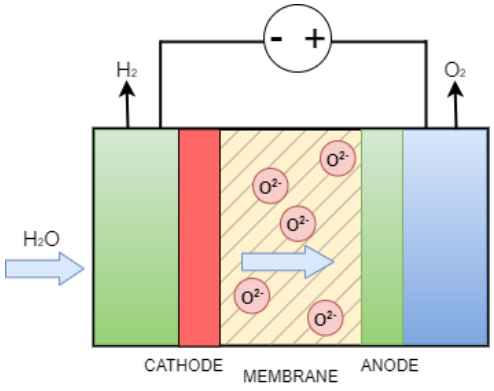

Figure 2.7: Solid Oxide electrolyzer

During the operation of the cell, the water steam is inserted in the cathode, where it is separated into hydrogen and oxide ions by the electrolyzing process which occurs in the cathode. The oxide ions are drawn through the ceramic membrane in the direction of the anode, where they will recombine and produce oxygen.

The reaction that occurs in the cathode is described as,

$$H_2O + 2e^- \rightarrow H_2 + O^{2-} \tag{2.12}$$

and at the anode side, oxygen is produced by the reaction,

$$2O^{2-} \rightarrow O_2 + 2e^- \tag{2.13}$$

SOE is a technology that is still in the process of development and is not yet commercially produced. Its main advantage is clearly the operation at high temperatures, which significantly reduces the voltage required for water electrolysis. However, system degradation is a drawback that must be considered [24].

2.2.3 Hydrogen storage system

A vast number of technologies have been proposed for hydrogen storage. One approach that has been utilized is the absorption of hydrogen in metals or chemical hybrids since hydrogen can interact with many substances. However, the most widely employed method currently is to store hydrogen in its gaseous or liquid state using physical storage [26].

Given the importance of fast access to pure hydrogen and efficient energy conversion, particularly for applications such as vehicle charging or supplying energy to the grid, physical storage methods have garnered significant attention within the energy sector. Therefore, in this work, we will focus on explaining the fundamental features of physical hydrogen storage.

Liquified Hydrogen

The process of storing hydrogen in its liquid state essentially involves cooling down the gas below its boiling point (-253 °C). In this state, hydrogen can achieve a volumetric density of around 71 kg/m^3, which is nearly twice as dense as its gaseous form at a pressure of 700 bars. The high volumetric density of liquefied hydrogen is its main advantage, particularly in applications with limited space, such as in vehicles.

However, this technology also comes with several drawbacks. The most evident one is the requirement for refrigerating the gas to a temperature much lower than the environment, which consumes a significant amount of energy, thereby decreasing the system's efficiency. The system is also susceptible to losses due to tank leakage, known as boil-off losses. Taking all these factors into account, it is estimated that around 40% of the injected energy is lost in the process of storing hydrogen using this method [18].

Compressed gas

The use of high-pressure tanks is the most well-established technology for hydrogen storage. This method dates back to the end of the 19th century when a steel vessel was

employed to store hydrogen at a pressure of 12 MPa. Today, this technology can be classified into four types of vessels commonly used for hydrogen storage, which are as follows [27]:

- Type 1: Fully metallic pressure vessels. These types are used in industrial and stationary applications due to their low density, which affects the tank's size and weight. The gas pressure in this scenario ranges between 15 to 30 MPa.
- Type 2: Metallic vessels with glass fiber composite reinforcement. These tanks can accommodate the highest pressure levels for hydrogen storage, reaching up to 100 MPa. Due to their high-pressure capabilities, they are also applied in stationary scenarios, such as fueling stations.
- Type 3: Vessels fully wrapped with a metal liner. These tanks operate at pressures ranging from 30 to 70 MPa and are typically used for on-board storage.
- Type 4: Fully composite vessels. These also operate at pressures up to 70 MPa. In this case, the tanks can be used for stationary low-pressure hydrogen storage or on-board storage systems.

Regarding hydrogen storage system methods, pressure tanks offer several advantages, and flexibility is one of them. Given the variety of technologies available, it is possible to adjust the system to different applications as needed. Storing hydrogen in its gaseous state also presents the advantage of being a rapidly deployable technology, as most applications require hydrogen in its gaseous form, and it can be easily transported.

2.2.4 Hydrogen fuel cells

Previously, it was detailed how electrolyzers were capable of producing hydrogen by using electricity and water. On the other hand, fuel cells perform the opposite operation; they generate electrical energy from hydrogen. In fact, as will be shown, the technologies applied to both of these processes are quite similar and are based on the same principles. This chapter will delve into some of the main concepts regarding fuel cell technologies.

A simple fuel cell is illustrated in Figure 2.8 and its operation can be described as two electrodes connected to an electrolyte solution, when hydrogen is introduced to the system, it becomes ionized, resulting in a current that passes through the electrolyte. This oxidation reaction takes place at the anode [28], and it can be described as follows:

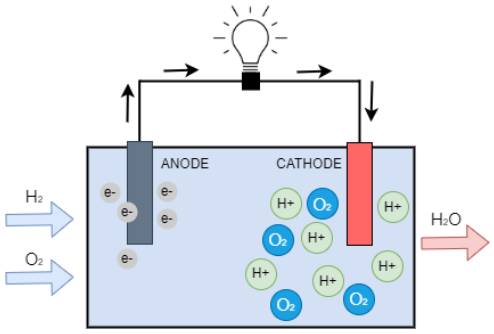

Figure 2.8: Hydrogen production methods

$$H_2 \rightarrow 2H^+ + 2e^- \tag{2.14}$$

The energy produced is a result of the oxidation of the hydrogen, as explained in the previous equation. However, this isn't the end of the process. Simultaneously with the introduction of hydrogen, oxygen is also injected into the solution. The molecules of oxygen combine with the products of the preceding reaction, leading to a reaction at the cell's cathode. This reaction is described as follows:

$$0.5O_2 + 2H^+ + 2e^- \rightarrow H_2O \tag{2.15}$$

Just like electrolyzers, fuel cells can be designed using various methods. Some of the main fuel cell technologies applied today include Polymer Electrolyte Membrane Fuel Cells (PEMFC), Solid Oxide Fuel Cells (SOFC), Alkaline Fuel Cells (AFC), phosphoric acid fuel cells, and Molten Carbonate Fuel Cells (MCFC) [29]. As mentioned previously, fuel cell technologies are quite similar to electrolyzers, and the terminology used to describe them depends on the type of electrolyte utilized in the cell. To avoid redundancy, this chapter will primarily focus on PEMFC methods, which will be the method applied in

this work.

Polymer Electrolyte Membrane Fuel Cell

In the PEM full cells, the electrodes are separated by a polymer membrane, which serves as the electrolyte medium of the system. The primary operation is quite similar to the one presented in the case of the simple fuel cell. The main difference is that the injected gases are kept separate, preventing side reactions that might occur in the system and thus increasing the overall efficiency. An illustration of a PEM fuel cell is provided in the Figure 2.9.

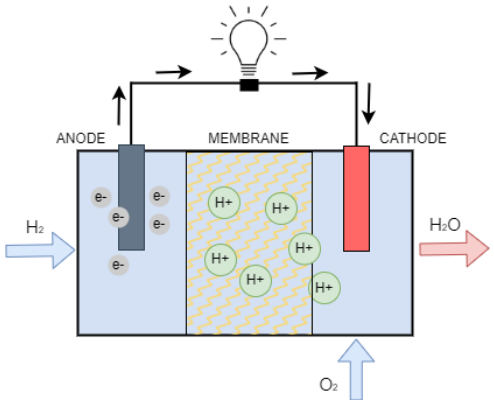

Figure 2.9: PEM fuel cells

Compared with other fuel cell technologies mentioned earlier, the PEM fuel cell offers several advantages that make it particularly attractive for use in power system applications. These advantages include its fast startup time, high power density, and high efficiency. Consequently, PEM fuel cells are considered a promising technology to be applied in transportation and stationary hydrogen-based devices [29].

2.2.5 Hydrogen storage system and power systems

As discussed earlier, the hydrogen economy has primarily been represented by its application in the chemical sector, such as refining petroleum and producing fertilizer. Factors like capital costs, technological limitations, and efficiency have prevented hydrogen from

becoming a relevant player in the energy market. However, the increased penetration of renewable energy into the electrical grid has created an opportunity to invest in clean and flexible methods for energy storage and conversion.

Regarding the application of hydrogen to support the electrical grid, it is often compared to battery banks used to increase grid flexibility, given their similar operational characteristics. Both systems have their advantages and drawbacks: HSS can provide energy as long as there is fuel to supply its fuel cells and have a shorter recharging time compared to battery storage systems. However, batteries present a lower capital cost and higher efficiency compared to HSS [30].

Several schemes for the application of HSS in power systems have been proposed. One system could incorporate only electrolyzers, offering a variety of options for the use of the produced hydrogen. Another approach would involve a complete setup of electrolyzers, storage tanks, and fuel cells. In this configuration, the system can store electrical energy and deploy it whenever it is more convenient for the grid [31].

A simplified representation of an HSS applied in a renewable energy scenario is presented in Figure 2.10. In this case, when there is an excess of energy production in wind power plants or solar power facilities, the electrolyzer can become active to convert some of the surplus energy into hydrogen. Conversely, if there is a shortage of energy production in renewable parks, the HSS can supply the grid with stored energy in the form of hydrogen.

In order to connect the HSS to the electrical grid, it is necessary to regulate its voltage level and its characteristics, since the fuel cells and electrolyzer operate in DC mode and at magnitudes lower than those supplied by the grid. For that reason, DC power converters are used between the HSS devices and the electric grid, as shown in Figure 2.10. These converters are also responsible for controlling the voltage supplied to these devices. This, in turn, regulates the production of hydrogen on the electrolyzer side and the consumption of hydrogen in the fuel cells. Consequently, the system's operation is highly flexible and capable of adapting to a wide range of load and generation scenarios [32].

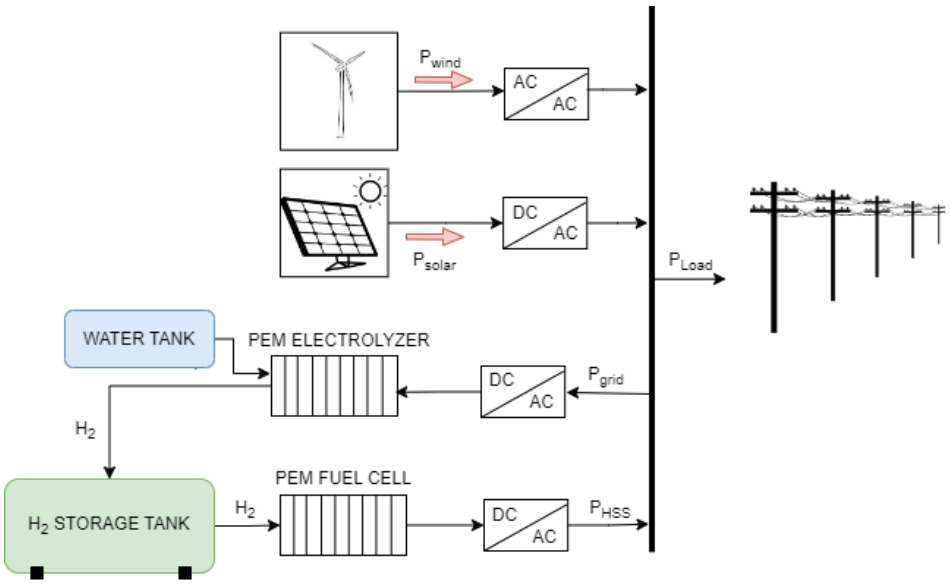

Figure 2.10: Hydrogen production methods

2.3 Summary

This chapter provides a contextualization of historical and technical concepts related to renewable energy curtailment and hydrogen-based technologies applied to storing and producing electrical energy.

The initial sections introduce the issue of increasing renewable energy curtailment worldwide, a consequence of the high penetration of RES generators in the grid. It also discusses some strategies created to mitigate this energy loss.

The following section delves into another important theme explored in this work: hydrogen storage systems. A brief historical contextualization of this theme is presented, followed by an examination of the technical aspects of hydrogen storage systems, including an explanation of the main components of this technology and their functionality.

Chapter 3

Optimal Power Flow

In a world where energy efficiency and the use of renewable sources are relevant topics, reliable and stable operation are not the only factors to be considered during power system planning. This transition is changing the dynamics of the electric networks and demanding the development of more complex models for representing the grid dynamics. Consequently, various methods are being introduced to address the problem of optimal operation and planning of the energy system.

In this context, the OPF algorithm is gaining significant relevance and is being applied in a wide range of applications. The OPF algorithm was initially introduced in 1962 by Carpenter in [33], and can be defined as a method to solve an optimal power dispatch problem. Later on, the algorithm had undergone variations, each possessing its own advantages for implementation in different scenarios.

Like standard optimization problems, OPF relies on a reliable model of the dynamics and behavior of the process to be optimized. In the case of analysis of the operation of the electric system, the power flow equations are usually used to represent the relationship between the variables of the electric grid, such as the bar's voltage and power injections [34]. However, the complexity of solving this problem due to non-linear relationships among variables makes it difficult to define an optimal solution, which sometimes may not even exist.

A method that is still widely applied involves using the simplified and linearized version

of power flow equations, known as DC-OPF. This method offers the advantage of being a convex problem that can be solved by linear optimization methods such as the simplex method [35]. However, current applications are demanding more accurate representations of the system to keep up with the expansion of the power grid and the connection of new electrical devices.

As a result, the OPF problem has become one of the most addressed problems in non-linear optimization. Deterministic algorithms for solving nonlinearly constrained problems like the Newton method and sequential quadratic programming (SQP) began to be applied in various applications in order to solve the OPF problem [36]. Furthermore, advancements in machine processing and the popularization of heuristic optimization methods led to more frequent implementation of these methods to address the non-convexity of the power flow problem. Nowadays, applications utilizing methods such as genetic algorithms, particle swarm optimization, and neural networks can be found quite often [37].

Another essential element in all optimization problems is the objective function. This can be described as a function determined by the variables of the OPF problem that is minimized or maximized according to the application, in order to attain the extreme value within the limitations of the problem under analysis. Examples of objectives frequently applied in OPF problems are the minimization of generation costs, minimization of transmission losses, and voltage quality at busbars [35].

Some analyses also employ multi-objective optimization methods to analyze different objective functions simultaneously. These methods utilize principles similar to single-objective approaches to achieve the optimal point. However, they differ in how they handle two or more objective functions, which can be managed by assigning weights to each one of the functions, as done in the weighted sum method, or by treating one of the functions as a constraint to be respected, as in the constraint method [38].

This chapter delves into the formulation and algorithms to solve the optimal power flow problem and its variations. First, the most widely used models for representing the dynamics of electrical networks and the state and control variables of this problem are presented. Furthermore, deterministic algorithms that have been implemented to solve

OPF are also explained. Finally, the multi-objective optimization methods are discussed.

3.1 OPF formulation

The standard OPF problem can be basically described as an optimization problem, where the variables are the states and control variables present in the formulation of the power flow of an electric network. Therefore, the problem can be described as followws,

$$\min \quad f(x) \tag{3.1}$$

$$s.t \quad g(x) = 0 \tag{3.2}$$

$$h(x) \leq 0 \tag{3.3}$$

in which $f(x)$ represents the objective function, $g(x)$ the equality constraints of the problem, and $h(x)$ the inequalities constraints [35].

3.1.1 Equalities constraints

In optimization problems, equality constraints can represent the model of the system under study. Similarly, in the classical OPF problem, equality constraints correspond to the power flow equations in the distribution network, also known as load flow equations [39].

The formulation of this model can be obtained from the relationship between the voltages and currents injected at the network's buses. Considering a network with n buses,

$$\begin{bmatrix} \dot{I}_1 \\ \dot{I}_2 \\ \vdots \\ \dot{I}_4 \end{bmatrix} = \begin{bmatrix} Y_{1,1} & Y_{1,2} & \dots & Y_{1,n} \\ Y_{2,1} & Y_{2,2} & \dots & Y_{2,n} \\ \vdots & \vdots & \ddots & \vdots \\ Y_{n,1} & Y_{n,2} & \dots & Y_{n,n} \end{bmatrix} \begin{bmatrix} \dot{V}_1 \\ \dot{V}_2 \\ \vdots \\ \dot{V}_4 \end{bmatrix} \tag{3.4}$$

being $\dot{V}_n$ and $\dot{I}_n$ the complex voltage and current at bus n, and $Y_{j,i}$ the admittance value between bus j and i. Taking into account that

$$\dot{I}_i = \frac{\overline{S_i}}{\overline{V_i}} = \frac{P_i - jQ_i}{\overline{V_i}} \tag{3.5}$$

in which $\overline{S_i}$ is the conjugate of apparent power, P_i, and Q_i represent the active and reactive power at bus i and $j = \sqrt{-1}$. Replacing Equation 3.5 in 3.4, and separating the real and imaginary terms, the relationship between the power injected in the bars and the magnitude and angle of the voltage can be described as [39],

$$P_i^{Gen} - P_i^{Load} = \sum_{k=1}^{N} |V_i||V_k||Y_{ik}|cos(\theta_i - \theta_k - \delta_{i,k}) \tag{3.6}$$

$$Q_i^{Gen} - Q_i^{Load} = \sum_{k=1}^{N} |V_i||V_k||Y_{ik}|sin(\theta_i - \theta_k - \delta_{i,k}) \tag{3.7}$$

where P_i^{Gen} and P_i^{Load} are the generated and consumed active power at bus i, Q_i^{Gen} and Q_i^{Load} are the reactive power generated and consumed at bus i, θ_i, and θ_k are the power angles in bus i and k and $\delta_{i,k}$ is the angle related to the branch admittance value.

The nonlinear characteristics of the electric network model, which can be noticed from Equations 3.6 and 3.7, are a challenge in solving the OPF problem. Furthermore, the problem is non-convex, which has led to an increase in the popularity of using heuristic algorithms to solve the OPF problem since they have a greater capacity to avoid local minima compared to deterministic algorithms [37].

3.1.2 Inequalities constraints

In an engineering optimization problem, the inequalities constraints usually represent the physical and security limitations regarding the problem approached. In the standard OPF problem, the same pattern can be noticed, and these inequalities represent the limitations of the devices within the electric grid, such as the maximum and minimum power flow through lines, bus voltage magnitude and angle, and the generator's active and reactive

power dispatch [34]. It can be represented as,

$$\theta_{min} \leq \theta_i \leq \theta_{max} \tag{3.8}$$

$$V_{min} \leq V_i \leq V_{max} \tag{3.9}$$

$$P_{min} \leq P_i \leq P_{max} \tag{3.10}$$

$$Q_{min} \leq Q_i \leq Q_{max} \tag{3.11}$$

$$S_{min} \leq S_{ik} \leq S_{max} \tag{3.12}$$

in which $S_{ik} = |V_i Y_{ii}|e^{j(-\delta_{ii})} + |V_i V_k Y_{ik}|e^{j(\theta_i+\theta_k-\delta_{ik})}$ and represents the apparent power through the lines.

3.1.3 Optimization methods

In this study, the focus will be mainly on methods for solving the standard formulation of the OPF problem. Therefore, this chapter does not contain formulations of algorithms to solve the DC-OPF or OPF that involve discrete variables. With that being said, some deterministic and heuristic methods that have been applied in power system optimization applications will be explored. Finally, the multi-objective approach to the optimization problem is discussed.

Newton's method

The Newton's method is a commonly used unconstrained optimization approach that has been employed to solve the OPF problem and is also integrated into other optimization algorithms, such as the interior point method, which will be approached later in this section. This technique is considered a deterministic optimization approach because it applies iteration methods using the gradient and Hessian of the objective function to guide it toward the optimal solution of the problem [34].

As mentioned, the Newton method is an unconstrained optimization approach. Therefore, to use it in the OPF problem, the objective function is extended to include the problem's constraints with penalty factors. This new function is known as the Lagrangian ($L(x)$) and can be defined as follows,

$$L(x) = f(x) + \lambda \sum_i g_i(x) + \mu \sum_j h_i(x) \tag{3.13}$$

in which λ and μ are the penalty factors of the equality and inequalities constraints, and $g_i(x)$ and $h_i(x)$ are the set of constraint functions. In this method, the inequalities constraints are only considered in 3.13 when they are active. After calculating the lagragian value, the algorithm proceeds to defining the search direction for the next iteration, which is calculated as,

$$S^k = -[H(x^k)]^{-1} g(x^k) \tag{3.14}$$

in which S^k is the search direction related to the iteration k, $H(x^k)$ the Hessian matrix of the Lagragion function and $g(x)$ is its gradient. After that, considering the use of a scalar step β^k , the variables for the next iteration are defined by,

$$x^{k+1} = x^k + \beta^k S^k \tag{3.15}$$

The last step during each iteration is verifying whether the algorithm tolerance was achieved. The methods used to check it are,

$$\frac{|L(x^{k+1}) - L(x^k)|}{L(x^k)} \leq \varepsilon_1 \tag{3.16}$$

or

$$||x^{k+1} - x^k|| \leq \varepsilon_2 \tag{3.17}$$

Figure 3.1 presents a step-by-step flow graph to solve the OPF problem using the

Newton optimization method.

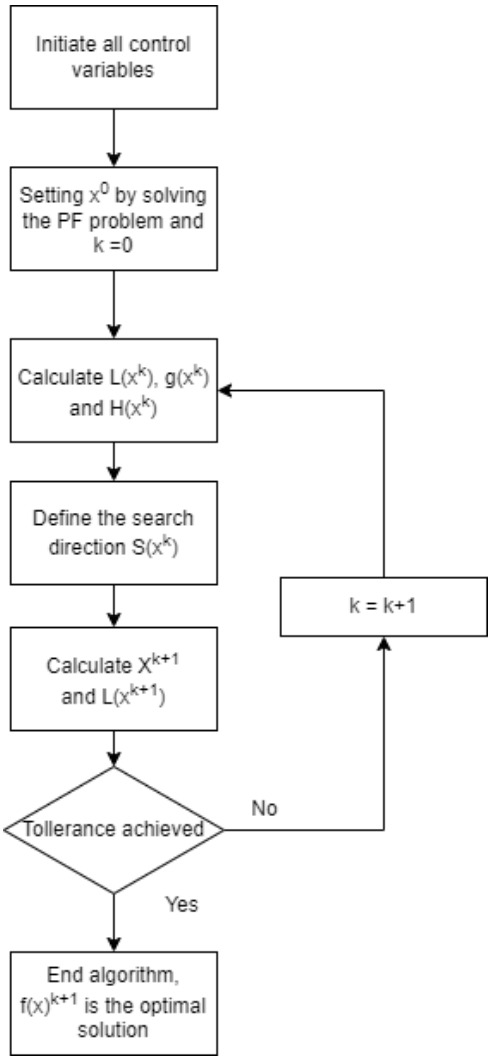

Figure 3.1: Flow graph of Newton algorithm applied in OPF

3.1.4 Interior Point Method

The interior point method (IPM) is also a numerical optimization method that has been widely applied to solve OPF problems. It is known for its ability to handle large-scale linear and nonlinear problems without the need of a large number of iterations. The algorithm's capacity to solve linear optimization problems and replace the simplex method was firstly presented by Karmarkar in [40], and due the success of this method, it was

later extended to deal with nonlinear problems as well.

The advantage of using the IPM over the standard Newton's is its capacity for dealing with inequality constraints even when they are not active. IPM utilizes barrier terms in the objective function to guarantee the feasibility of the problem by guiding the iteration solution to a trust region and increasing the penalty when the algorithm approaches the limits of the constraints [34].

One common barrier function is the logarithm function; in this case, the Lagrangian function of the IPM can be described as,

$$L(x) = f(x) + \lambda \sum_{i} g_i(x) + \mu \sum_{j} ln(h_i(x)) \tag{3.18}$$

where μ is the scalar that decreases to zero as each iteration of the problem is solved.

3.1.5 Active-set method

Another method used to handle the complexities of inequality constraints in nonlinear optimization problems is the Active-set method. In this case, as the name suggests, the algorithm will identify the active constraints during the iteration in order to consider only them when solving the optimization problem, consequently reducing the problem to one containing only equality constraints [41].

The main advantage of using the active set method is its ability to simplify the problem. In addition to eliminating the inequality constraints, which reduces the number of equations and variables to be analyzed in general, it makes the problem computationally more efficient, especially in cases that involve a relatively high number of inequalities. In [42] is presented the comparison of IPM with an active set in solving an OPF problem with a 14 bus network in which the latter was twice faster in some situations.

Active-set methods are used in various types of optimization problems, both linear and nonlinear. Regarding nonlinear applications, which include the OPF, a known method is the SQP, which is formulated as,

$$\min_{x} \ \frac{1}{2}x^T Hx + G^T x \tag{3.19}$$

$$s.t \ \ g(x) = 0 \tag{3.20}$$

$$h(x) \leq 0 \tag{3.21}$$

The standard problem is well known and the solution can be easily defined or it can be determined if it exists. In order to deal with the nonlinear characteristic of the OPF problem, the objective function is linearized and the problem is iterated until it converges to the optimal solution. The large number of constraints present in the OPF makes the Active-set method interesting to be applied in this case. Unlike the IPM, it will only consider the constraints that are necessary during the current analysis, significantly improving the performance of the problem [43].

3.2 Multi-objective optimization

The previous section presents some methods applied to solving the OPF problem considering one defined objective function. However, in power system applications, it is common to evaluate more than one objective, since efficient and secure operation can depend on multiple factors. Some of these objectives may impact each other, sometimes even competing, making it impractical to optimize each function individually. In such scenarios, it becomes necessary to introduce multi-objective optimization methods to simultaneously evaluate all objectives.

In this section, it is presented an overview of some necessary concepts in multi-objective optimization and techniques used for analyzing and solving multi-objective optimization problems (MOOP).

3.2.1 Methods for solving MOOP

Before delving into the algorithms used to deal with MOOP, it is necessary to explain some terms that arise when solving these problems. First, is the concept of dominance. The term is used during the comparison between two or more points in the set of solutions of an optimization problem. In general, one point is dominant over the other if it is more optimal considering the objective of the problem [44].

In single-objective scenarios, the dominance can be easily spotted as the point that is closer to the best solution of the problem in relation to another point. The term becomes more complex in MOOP, since in this case there will be multiple objectives, and the idea of dominance must include each one of the objectives analyzed.

In general, in multi-objective and single-objective problems, a solution point (x_1) is only considered dominant over another point (x_2) when,

$$f_i(x_1) \leq f_i(x_2) \qquad \text{for all } i \tag{3.22}$$

$$\text{and} \quad f_i(x_1) < f_i(x_2) \qquad \text{for some } i \tag{3.23}$$

being f_i the objective function i in the set of objective functions used in the problem.

As can be noticed by Equations 3.22 and 3.23, in single-objective approaches, only one point can satisfy both conditions; however, when dealing with MOOP, a set of dominant points can be generated, and it is denominated as a Pareto set, this is another important concept in multi-objective problems. Therefore, solving an MOOP can be described as defining the most suitable solution point in the Pareto set. Some of the methods used for defining this solution are presented hereinafter.

Constrain method

One possibility for solving a multi-objective problem is to optimize referring only to one of the objective functions and considering the rest as constraints of the optimization problem. This is known as the constraint method [38]. In this case, the objective problem

could be described as

$$\begin{aligned} \min \quad & f_1(x) && (3.24)\\ s.t \quad & f_2(x) \leq c_2 && (3.25)\\ & f_3(x) \leq c_3 && (3.26)\\ & \vdots \\ & g(x) = 0 && (3.27)\\ & h(x) \leq 0 && (3.28) \end{aligned}$$

in which c_1 and c_2 are parameters related to the maximum value allowed for the objective function $f_2(x)$ and $f_3(x)$. After defining these values, the problem can be approached by any method used for solving optimization, such as the ones presented in the previous section.

Weight methods

The weight method is the most intuitive method explained in this section. In this case, the MOOP is approached by assigning weights for each of the objective functions for then analyzing them simultaneously. The simplest way for analyzing the objective functions is by summing each function multiplied by its own weight [44]. In this case the objective problem is described as follows,

$$\begin{aligned} \min \quad & \mathbf{w} \cdot \mathbf{f}(\mathbf{x}) && (3.29)\\ & s.tg(x) = 0 && (3.30)\\ & h(x) \leq 0 && (3.31) \end{aligned}$$

Here, $\mathbf{w}$ represents the vector containing the weights for each objective. Another advantage of using weight-based methods is their simplicity in generating the Pareto

front. However, the sum weight method can only represent linear relationships between objective functions. To represent non-convex characteristics, it is necessary to apply different weight methods [38].

Population methods

Another method of defining the Pareto front of an optimization problem is to use population algorithms. These algorithms have great advantages in searching the solution space, reaching points that can be overlooked by the standard deterministic approaches, and also the capacity for analyzing a great number of solution points simultaneously.

In order to define the dominant points, the population algorithms can be improved in order to generate subpopulations that are designed to pay higher attention to one specific objective, delete non-dominant points, or rank the points closer to the Pareto front in order to give them advantages in the next generation. The NSGA-II is an example of a populational multi-objctive optimization algorithm that has been highly employed [45].

3.2.2 Goal attainment method

In this study, the MOOP will be solved by using the method known as the goal attainment method, also referred to as goal programming. The approach was first introduced by Genbicki in [46], and it was improved with the study of different tequinics for implementing it in optimization problems, in [47] is presented some variations that were developed.

Among these variations, the method explained in this section is known as the Weighted Min-Max method [47]. It has been successfully applied in OPF applications and has demonstrated superior performance compared to population-based methods [48]. The Goal Attainment method essentially involves minimizing the deviation between the objective function value and the desired goal value, with weights used to scale the impact of each objective function. In this scenario, the MOOP can be described as follows,

$$\min_{x,\gamma} \ |\gamma| \tag{3.32}$$

$$s.t \ \ f(x) - w \cdot \gamma \leq \text{goal} \tag{3.33}$$

$$g(x) = 0 \tag{3.34}$$

$$h(x) \leq 0 \tag{3.35}$$

where γ represents the vector containing the deviation of the objective function to its utopia value and w the weight vector.

Just as in the other methods presented in the previous section, after applying the goal attainment formulation, it is possible to solve the MOOP by the use of any of the single objective optimization methods, of course, according to the algorithm limitations. Furthermore, the optimal solution will depend on the weight defined for each objective function; therefore, it should be carefully chosen.

The advantage of using the Weighted Min-Max Goal Attainment method is its ability to generate a comprehensive Pareto front, which includes scanning non-convex solution curves. The only drawback is that the method will also include weakly Pareto fronts, as will be demonstrated in the results section [38].

Generating the Pareto front

By applying different weight values, a Pareto set containing many optimal solutions for the problem can be generated [48]. First, considering that w_1 and w_2 represents the weight of the first and second objective function respectively and that $\mathbf{w} = [w_1, w_2]$, is a matrix containing all weight values regarding both objective functions and considering that the problem will be evaluated in N different weight scenarios, the points that compose the Pareto set are defined as,

$$J_{pareto} = \begin{bmatrix} J_1^{w(1)}, & J_2^{w(1)} \\ \vdots & \vdots \\ J_1^{w(N)}, & J_2^{w(N)} \end{bmatrix} \tag{3.36}$$

where $J_1^{(N)}$ and $J_2^{(N)}$ are the optimal solution of the objective functions 1 and 2, considering the weights value located in the N line of $\mathbf{w}$ variables. w_1 and w_2 are defined as,

$$w_1(j) = \frac{j}{N}$$
$$w_2(j) = 1 - \frac{j}{N}$$

for $j = [1, 2 \ldots N]$.

3.3 Summary

This chapter presents a brief contextualization and formulates some of the methods for solving the OPF problem, considering single- and multi-objective optimization problems. It also explains the notion of the Pareto front and a process that can be used to generate it.

First, it provides an overview of the history and current status of the OPF problem, citing the modifications it has undergone and the new methods being applied to solve it.

The chapter then proceeds to present the formulation of the OPF problem. In this section, mathematical models of the electric grid are introduced, along with the format of the optimization problem, composed of the objective function, inequality constraints, and equality constraints.

Following this, three optimization methods for solving the single-objective OPF problem are presented: the Newton method, Interior-point method, and Active-set method.

Finally, multi-objective optimization problems are discussed, including an explanation of important terms related to MOOP, the formulation of the goal-attainment method, and

a method for generating the Pareto front using this approach.

Chapter 4

Case Study

As previously mentioned, the core purpose of this study is to introduce a multi-objective approach designed to optimize the dispatch of renewable generation within an electric grid. In order to perform such analyses, it is necessary first to construct practical scenarios that can be used to simulate real-world situations. This chapter aims to present the methods used to generate these scenarios.

Initially, the physical aspects of the electrical grid used in this case study are presented. This includes defining the topology of the grid, the load and generation profiles, specifying the grid parameters, and outlining the characteristics of the incorporated hydrogen storage system, which is implemented in some of the cases analyzed.

Subsequently, the multi-objective approach applied to solve the OPF problem is explained, and constraints are imposed on certain variables, such as voltage magnitude and power angle, power flow through lines, and active and reactive power of generators. Another pivotal point is the strategy utilized to effectively handle the curtailment of active power in RES sources. In this chapter, the strategy utilized to effectively handle the curtailment of active power in RES sources is presented. This curtailment will be enforced as a constraint within the scope of the OPF problem.

4.1 IEEE 14 bus example grid

The IEEE 14-bus grid is a simplified representation of the American electrical grid in 1962. Most of its characteristics are presented in [49], which makes it very practical for simulating hypothetical scenarios. In fact, there are a large number of academic works that employed this system for power system analysis. IEEE 14-bus electrical grid is illustrated in Fig. 4.1.

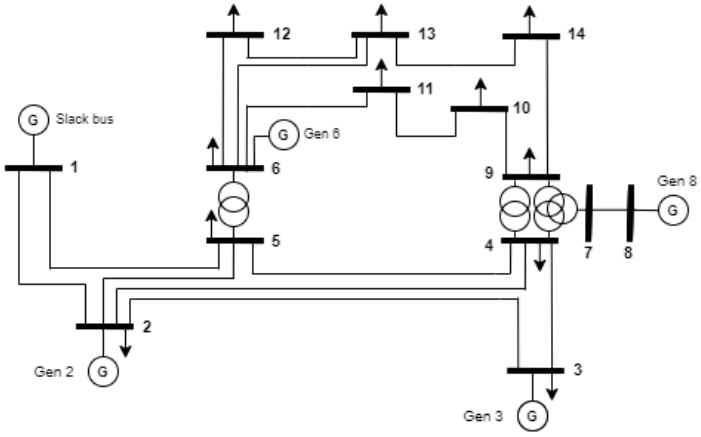

Figure 4.1: IEEE 14-bus network

As illustrated in the Figure 4.1, the grid consists of 5 generators, 11 loads, and 20 lines, of which 3 of them are connected to transformers. The following section will detail how the generation and load for each bus were defined for each of the scenarios approached.

4.2 Load and Generation

Since the objective is to obtain results for a year-long grid operation, conducting an individual OPF analysis for each hour of the year would be impractical. Therefore in order to represent the whole year's operation, four cases were designed, each one representing a day of a season of the year. The cases are outlined as follows:

- Case 1: Represents Spring: February, March, and April
- Case 2: Represents Summer: May, June, and July

- Case 3: Represents Autumn: August, September, and October
- Case 4: Represents Winter: November, December, and January

Afterward, the OPF will be analyzed hourly, considering that each case will be examined successively from 1 to 4. This methodology is necessary, especially during scenarios in which the HSS will be considered in the simulations.

Load

Since the IEEE 14-bus network documentation only presents the grid's fixed operational values of load and generation, it becomes necessary to construct load curves for each bus, capturing their changes throughout the day. In order to achieve a more realistic representation of load behavior, a dataset of real residential and industrial loads was used to create the load profiles. The dataset presents hourly load data during a year of simulated buildings adapted to the state of New Jersey, the data is available from [50].

To design the load dynamics for each bus, four possibilities for the load profile were considered. The bus could have a fully industrial profile (100% industrial), a predominantly industrial profile (80% industrial and 20% residential), a predominantly residential profile (20% industrial and 80% residential), or a fully residential profile (100% residential), considering the data-set presented previously. Using this framework, the load for each bus was defined and scaled according to the original load values presented in the documentation.

Finally, to generate the four scenarios, the dataset was partitioned based on the seasons of the year. An illustrative day for each season was then constructed by computing the average load value for each hour of the day.

Generation

The original IEEE 14 bus network does not include any RES generators; therefore, the generators located on buses 3, 6, and 8 were replaced by a 100 MW capacity wind power plant and 70 MW and 100 MW capacity solar power plants, respectively. Regarding

the generator located at bus 2, it was considered a conventional synchronous machine generator with 40 MW capacity with the assignment of supply energy during the shortage, but mostly, compensate for the reactive power of the system.

At last, bus 1 was defined as the slack bus, which is necessary to set a common voltage magnitude value and its power angle. The slack bar also represents the connection with an external grid, the exchange between these grids will not be limited, however, this energy will be analyzed as non-beneficial to the grid since represents a lack of autonomy of the grid. This will be further approached during the Results section.

The generation profiles for each power plant connected to the electrical grid demands the same procedures as the load profiles. It is necessary to model these generators in order to obtain dynamic behaviors for each hour that will be analyzed. However, at first, it is necessary to define the type of generation that will be produced on each bus.

Wind power generation Many variables can influence wind power generation, including wind speed, temperature, wind direction, and turbine conditions. However, for the purpose of this work, we focus on wind speed as the only determinant of wind power plant generation. This choice is a reasonable approximation when we are dealing with large-scale production and slow dynamics monitoring.

A simplified model representing the power output of a wind turbine (P_{wind}) can be represented as follows [51]:

$$P_{wind}(v) = \begin{cases} 0, & v \leq v_c \text{ or } v \geq v_f \\ P_r(\dfrac{v - v_c}{v_r - v_c}), & v_c \leq v \leq v_r \\ P_r, & v_r \leq v \leq v_f \end{cases} \tag{4.1}$$

in which P_n is the turbine's rated power, v_r the rated velocity, v_c is the cut-in velocity, v_f

the cut-off velocity and v the wind velocity measured at the moment.

In order to define these parameters, it is necessary to understand the operational conditions of the turbines used for energy generation. For the purpose of this work, it was assumed that the wind power plant would consist of turbines of the Vestas V100 - 2.0 MW model [52]. Table 4.1 describes some of the characteristics of the turbine utilized.

Table 4.1: Vestas V100 - 2.0 MW wind turbine [52]

Parameters	Value
Rated Power	2 MW
Rated velocity	12 m/s
Cut-in wind speed	3 m/s
Cut-out wind speed	22 m/s
Hub height	95 m

By substituting the parameters presented in Table 4.1 into Equation 4.2, it becomes feasible to construct a model for the power generated by the wind turbine and, consequently, for the entire power plant. This allows us to determine how power production will vary during each scenario based on current wind speed.

Wind speed profiles for each representative day of the year were constructed using data collected from the Open-Meteo website [53]. This dataset comprises five years of hourly wind speed data from a location near the city of Faro, Portugal, from 2016 to 2020. This location was selected due to its high average wind speeds, a critical factor for the wind power plant.

After that, the data were categorized according to the corresponding season in which it was collected, and these sets were utilized to develop a probabilistic model for the seasonal wind speed in the region. The Weibull probabilistic density function stands as the most commonly employed model for describing wind speed behavior in a specific location and can be defined as follows [54],

$$f_w(v) = \frac{k}{c}(\frac{v}{c})^{k-1}e^{-(\frac{v}{c})^k} \tag{4.2}$$

in which c and k are parameters known as scale and shape index, respectively. In Figure

4.2 displays the comparison between the wind velocity occurrence in each season and its respective Weibull model.

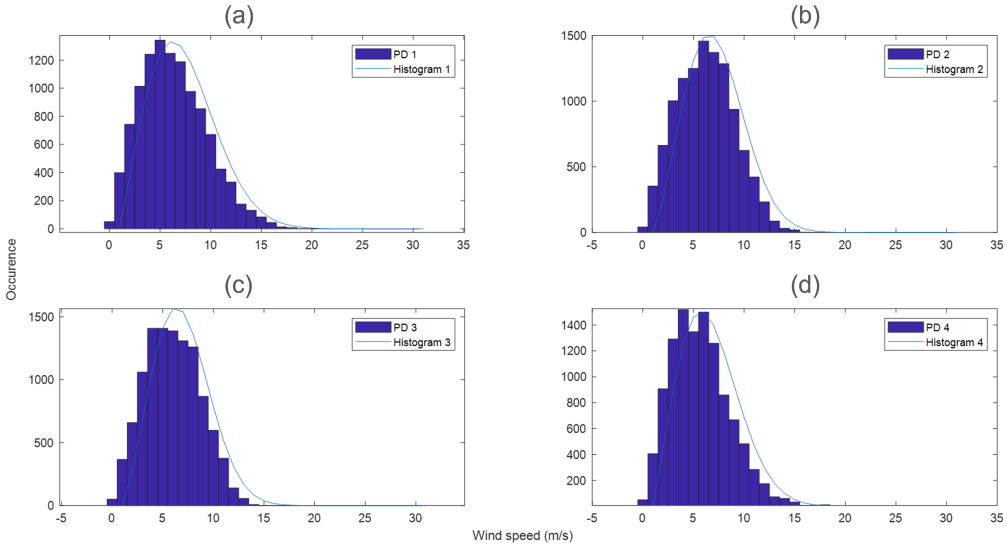

Figure 4.2: Wind speed histogram compared to Weibull model (PD). (a) Spring (b) Summer (c) Autumn (d) Winter

Using the Weibull model, it becomes possible to create an hourly wind velocity profile for each representative day and consequently determine the power generation of the wind power plant during each hour using Equation 4.2.

Photovoltaic generation The generation of the solar power plant was defined in a similar manner to that used for wind generation. The model for photovoltaic panel generation is simplified by considering irradiation as the major factor affecting the power supply for the solar park. Therefore, the power extracted from the solar PV system (P_{pv}) can be defined as follows,

$$P_{pv}(G) = \eta \cdot S \cdot G \tag{4.3}$$

in which η represents the overall efficiency of the system, S the surface area of the modules, and G the irradiation at the moment.

The irradiation curves for each scenario will also be constructed based on the dataset

collected from the website Open-meteo, which provides five years of hourly irradiation data for the same location in which the wind speed data was collected. Similarly, the data were classified into four sets corresponding to each season. The hourly irradiation for each representative day in each scenario was determined by calculating the mean values of the data set for the respective hour of the day.

4.2.1 Profile of load and generation

Figure 4.3 presents the hourly load and RES generation profiles considering each representative day as explained earlier, from Case 1 to Case 4. This scenario serves as an interesting case study for this work because the generated energy occasionally exceeds the load. This provides opportunities to optimize energy dispatch either by dispatching to the slack bus, activating the storage system, or curtailing this energy. Additionally, Table 4.2 provides a summary of the composition of generation and load buses on the grid.

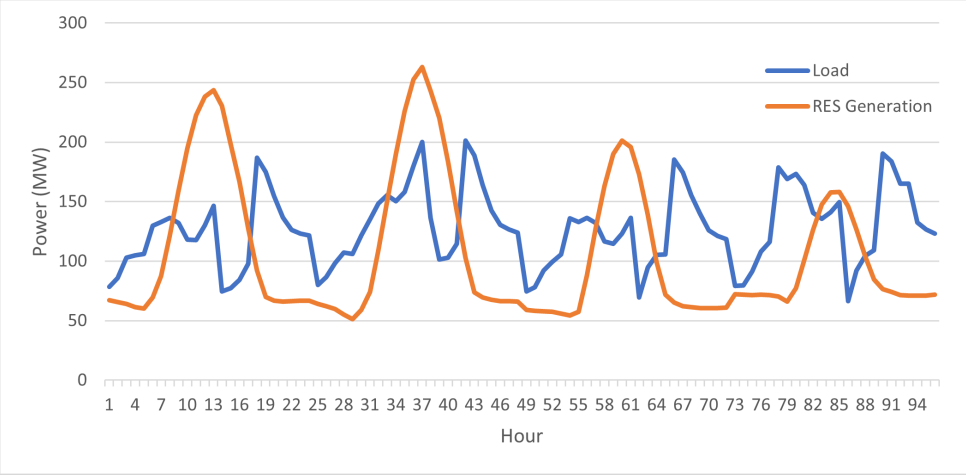

Figure 4.3: Total Load and RES generation during the four representative days

4.3 Hydrogen Storage System

This section introduces the models and methods employed in order to include the hydrogen storage system (HSS) in the OPF problem. In this work, the main objective of using

Table 4.2: Description of each bus in the power grid

Bus	Status	Generation profile	Load profile
1	Slack bus	External grid connection	None
2	PV	Synchronous machine	Fully industrial
3	PV	Wind Park + HSS	Fully residential
4	PQ	None	Fully residentia
5	PQ	None	Fully residential
6	PV	Solar park 1	Fully industrial
7	PQ	None	None
8	PV	Solar park 2	None
9	PQ	None	Predominantly industrial
10	PQ	None	Fully industrial
11	PQ	None	Predominantly industrial
12	PQ	None	Predominantly residential
13	PQ	None	Predominantly residential
14	PQ	None	Predominantly industrial

an energy storage system is to mitigate renewable energy sources (RES) curtailment and improve the grid's autonomy by minimizing energy exchange with the slack bus. Furthermore, in this study, the stored hydrogen level will also be used to define the optimal solution for the multi-objective problem. This concept will be further explained later in this chapter.

As discussed earlier, the HSS consists of three main components: the electrolyzer, the hydrogen storage tank, and the fuel cells. Each of these devices operates differently and should be taken into account for proper integration into the OPF problem. In this section is explained how each device was designed to be incorporated into the electrical grid under study.

4.3.1 Electrolyzer

As mentioned earlier, the electrolyzer is linked to the grid through a power inverter, which reduces the grid voltage to match the requirements of the electrolyzer cell and regulates the power injected into the electrolyzer.

The mass of hydrogen produced by the electrolyzer ($M_{H_2}^{prod}$) can be calculated as [55],

$$M_{H_2}^{prod} = \frac{\mu_{Ele} I_{cell}}{2 \cdot F} \tag{4.4}$$

in which μ_{Ele} is the cell's electric efficiency, I_{cell} the current through the electrolyzer, and F the Faraday constant.

By analyzing the equation 4.4 is possible to notice that hydrogen production is directly related to the current injected in the electrolyzer. This characteristic, along with the control of the cell's voltage, allows a very flexible operation of the fuel cell, which can be set for different rates of hydrogen production.

In order to ensure a more accurate operation of the HSS, real devices available in the market will be employed to design the system. For electrolyzer cells, the Nel Hydrogen MC500 model will serve as a reference [56]. The MC500 is a hydrogen generation system consisting of a PEM electrolyzer. The characteristics of the system are detailed in Table 4.3.

Table 4.3: Nel Hydrogen - M-serie MC500 hydrogen generation system [56]

Parameters	Value
Hydrogen production rate	492 Nm^3/h 44,25 kg/h
Power consumption per volume H_2 produced	5,1 kWh/Nm^3
Maximum power consumption	2,5 MW
Start-up time	$\leq$ 8 min
Ramp-up	$\leq$ 15 sec

The hydrogen generation system start-up and ramp-up time are very short and, therefore, it should not influence the hourly hydrogen production. Regarding the efficiency of this system (η_{ez}), it can be calculated by [55],

$$\eta_{ez} = \frac{HHV \cdot M_{H_2}^{el}}{E_{el}} \tag{4.5}$$

being HHV the high level-heat of hydrogen and E_{el} the energy needed to produce the mass of hydrogen $M_{H_2}^{el}$ (kg). Using the data presented in Table 4.3, the device has a

hydrogen production rate of around $17,7$ kg/MWh, replacing this value in Equation 4.5 and considering HHV of 39.39 KWh/kg, the efficiency can be defined as $\eta_{el} = 0,697$.

4.3.2 Hydrogen storage tank

Similar to electrolyzers and fuel cells, storage tanks also include additional devices necessary for performing specific tasks within the system. Examples of these devices are the water storage tank, oxygen storage tank, and pressurizer. Just like power converters, it will be considered that these devices do not interfere with energy management.

The hydrogen tank considered as a model for this study is also a device supplied by the company Nel Hydrogen, known as the Hydrogen Storage 20MPa - SS001 [56]. This technology features a type 1 steel tank with the capacity to store 500 kg of compressed hydrogen. An illustration of the storage rack can be seen in Fig. 4.4. Finally, the losses in storage will be considered insignificant compared to those in energy conversion.

Figure 4.4: Neo hydrogen's steel tank [56]

4.3.3 Fuel Cell

The fuel cell is the device that will generate energy back to the grid using the hydrogen that was stored previously. The device also employs power converters in order to connect the system to the electrical grid and regulate the current supplied to the cell.

The device used as a model in this work is the ClearGen II model supplied by the company Ballard [57]. This model was chosen due to its high capacity, making it suitable

for operation in a stationary storage system. The main characteristics of this device are described in Table 4.4.

Table 4.4: Ballard ClearGen - Hydrogen Fuel cell generator [57]

Parameters	Value
Net power	1 MW
Fuel consumption	63 kg/hr

In order to calculate the efficiency of the device (η_{FC}), the following equation was used [55],

$$\eta_{FC} = \frac{E_{FC}}{LHV \cdot M_{H_2}^{FC}} \tag{4.6}$$

where E_{FC} represents the energy injected in the grid, LHV the hydrogen lower heating value, and $M_{H_2}^{FC}$ the mass of hydrogen consumed in the process. Replacing the value of the parameters and the value known by the device specification, $\eta_{FC} = 0,48$.

4.3.4 Hydrogen storage system operation

The flexible operation of the electrolyzer and fuel cell allows us to consider these devices as an additional load and generator, in the case of the electrolyzer, inserted in the power grid. In this manner, the power consumed or injected into the HSS will be optimized according to the objective function applied in the analyses. The constraints that limit the behavior of the maximum power consumption and production by the HSS and the hydrogen level stored in the hydrogen tank are considered as,

$$-P_{ez}^{max} \leq P_{ez} \leq -0.1P_{ez}^{max} \tag{4.7}$$

$$0 \leq P_{FC} \leq P_{FC}^{max} \tag{4.8}$$

$$L_{H_2} \leq L_{H_2}^{max} \tag{4.9}$$

being P_{ez} and P_{FC} the electrolyzer power consumption and the Fuel cell electric power

generation, respectively, and L_{H_2} is the hydrogen stored in the pressure tank.

Regarding the hydrogen stored in the pressure tank (L_{H_2}), the level of hydrogen will be calculated as,

$$L_{H_2}(t+1) = L_{H_2}(t) + e_{el} \cdot \eta_{el} \cdot P_{ez}(t) - e_{FC} \cdot \frac{P_{FC}(t)}{\eta_{FC}} \tag{4.10}$$

which e_{el} and e_{FC} represent the state of the devices, either on (1) or off (0) states. Since the HSS is applied to reduce energy curtailment and improve grid flexibility, it is illogical for both the electrolyzer and fuel cells to operate simultaneously. This would imply a circular operation of the system, resulting in a waste of energy.

Another restriction that is being considered and that may not be so obvious as the previous one, is that the e_{el} is only activated in the case that the energy produced by all generators is greater than the load of the system. Otherwise, the system could request the energy from the slack bus to produce hydrogen, which is not the objective of this work.

Considering the example devices presented earlier, certain characteristics of the hydrogen storage system (HSS) to be integrated into the power system have been defined and are presented in Table 4.5. However, this study does not deal with the optimization of the size or positioning of the HSS components. The rated power of the electrolyzer and the fuel cells were determined based on the installed generation capacity of the system. Additionally, the hydrogen storage tank's size was designed to stand approximately twelve hours of the electrolyzer's nominal operation. Concerning the placement of the HSS, it was set at bus 3 of the power grid. This decision was made due to the wind power park's location at this particular bus, which is the grid's main energy producer.

Table 4.5: Rated characteristic of HSS

Device	Parameters
Electrolizer power consumption	50 MW
Fuel Cell's net power	50 MW
Storage tanks's capacity	10000 Kg

4.4 Renewable energy curtailment specification

An important aspect of this work is the evaluation of the active power curtailed at the RES generators. As approached earlier, the European regulation on the internal market for electricity established that the maximum annual energy curtailed in RES generators should not exceed 5% of the total energy generated by the same power plant. Furthermore, such events should be decided in a non-discriminatory manner.

In this research, the method proposed to deal with the curtailment in the power grid is to add the following constraints in the OPF problems, ensuring that the system operation will occur within the limitations that were determined.

Regarding the total renewable energy curtailment (E_s) limitations, the constrain added to the OPF problem is defined as,

$$E_s = \frac{\sum_{k=0}^{T}(P_s^{max}(k) - P_s(k))}{\sum_{k=0}^{T} P_s^{max}(k)} \leq 0.05 \tag{4.11}$$

in which $P_s^{max}(k)$ the maximum capacity of production at the moment k, $P_s(k)$ is the dispatched power at the moment k and $s \in \{3, 6, 8\}$, representing the buses with RES generators.

The discrimination among the generators (D) will be analyzed by calculating the standard deviation of the energy curtailed at each of the generators located in s. In order to enforce a lower value for this variable, a new nonlinear constraint is added to the problem,

$$D = \sqrt{\frac{\sum_{i \in s}(E_i - M_s)^2}{N_s}} \leq 0.01 \tag{4.12}$$

where M_s represents the mean of the total energy curtailed among the RES generators and N_s is the number of RES generators in the grid. In this work, the upper bound of the discrimination profile was considered to be 1%, as shown in the Equation 4.12.

4.5 Optimization problem formulation

So far, this chapter has explained how each of the devices present in the power grid and some other aspects, such as energy curtailment, will be represented and modeled in the energy optimization problem. These mathematical concepts are very important to obtain a complete representation of the electrical grid studied in this work.

This section will present which optimization method will be employed during each scenario, and how they will be used to obtain the expected results for the final analyses. In addition, the multi-objective approach for the optimization will be explained and detailed.

The scenarios that will be analyzed in this work can be divided into: single-objective optimization problem without energy storage, multiobjective optimization problem without energy storage, single-objective optimization problem with energy storage, and multiobjective optimization problem with energy storage.

However, in order to avoid any confusion that may arise while evaluating these different scenarios simultaneously, at first the impact of the multiobjective approach will be analyzed without the implementation of the HSS. After that, the same optimization methods will be employed in order to analyze the inclusion of the energy storage system in the power grid and its impact on energy management. At last, the multiobjective optimization problem will be evaluated with the application of the HSS. These three analyses are approached in the next chapter by the denomination of (1) Multi-objective approach analysis, (2) Energy storage system analysis, and (3) Multiobjective approach with energy storage analysis.

4.5.1 Objective functions

The two objective functions used in this work are (1) the minimization of transmission losses and (2) the minimization of active power curtailment in RES generators. To implement these objectives in the OPF problem, it is necessary to express them in terms of the variables used in the power flow equation, as mentioned earlier. The total transmission loss (P_{loss}) in the power grid can be described as [48],

$$P_{loss} = \sum_{k,m \in N} \frac{R_{k,m}}{R_{k,m}^2 + X_{k,m}^2}(V_k^2 + V_m^2 - 2V_k \cdot V_m \cdot cos(\delta_k - \delta_m)) \tag{4.13}$$

in which $R_{k,m}$ and $X_{k,m}$ represent the resistance and inductive reactance parameters of the line between the buses k and m.

The active curtailment (C_{total}) is being calculated as,

$$C_{total} = \sum_{i \in s}(P_s^{max}(k) - P_s(k)) \tag{4.14}$$

Therefore both objective functions considered in this study are,

$$f_{obj}^1 = \min P_{loss} \tag{4.15}$$

$$f_{obj}^2 = \min C_{total} \tag{4.16}$$

Although it may not be obvious by the mathematical description, the relation between these two objective functions is inverse, which means that minimizing one of them will normally decrease the other, this relationship is demonstrated further in this work in the Results chapter.

4.5.2 Constraints description

Table 4.6 it is shown all the lower and upper limits of the constraints applied in the OPF problem. These values will not change during different scenarios, only the minimum and maximum values regarding the power dispatch by RES generators, which are updated each hour.

4.5.3 Multiobjetive optimization approach and Pareto front

The inverse relation between both objective functions chosen in this work makes the application of the multiobjective optimization approach interesting in order to evaluate

Table 4.6: Values of OPF inequality constraints.

Variables	Lower bounds	Upper bounds
V_i (p.u)	0.95	1.05
δ_i (°)	-60	60
S_{ik} (p.u)	–	1.0
P_2 (p.u)	0.4	0.4
Q_2 (p.u)	-0.4	0.5
P_s (p.u)	$0.95 \cdot P_s^{max}$	P_s^{max}
L_{H_2} (kg)	0	10000
P_{ez} (MW)	5	50
P_{FC} (MW)	-50	0
D	–	0.01

different optimal solutions that can be considered to solve the OPF problem. To conduct such analysis, a common method used in multiobjective optimization is using the Pareto front, which consists in generating a set of solutions located on the border of optimality of both objective functions in order to achieve interesting insights about the problem.

The algorithm applied for the multi-objective optimization approach in this work is the goal attainment method. The approach enables the generation of a Pareto set of each analyzed OPF problem, simply by varying the weight of the objective function, as explained in Section 3.2.2.

After obtaining the Pareto set of solutions, the question that arises is how to define the optimal fit solution for that given scenario. In general, by generating the Pareto front, the problem can be handled, so each researcher can define the best way to decide the optimal solution point. In this work, two methods for defining the fittest solution are proposed for each case. The first one will be approached in the cases without energy storage and the second with the cases which present energy storage.

The first approach was defined considering that the fittest point would be a trade-off between both objective functions, by defining $J_{Pareto}(j_{fit})$. as the optimal point to the scenario, j_{fit} is computed as

$$j_{Fit} = arg\min_{j}(J^{Norm}_{Pareto}(j,1) + J^{Norm}_{Pareto}(j,2)) \tag{4.17}$$

in which J_{Pareto}^{Norm} represents the normalized vector J_{Pareto}, calculated by,

$$J_{Pareto}^{Norm}(j,n) = \frac{J_{Pareto}(j,n) - J_{Pareto}^{min}(n)}{J_{Pareto}^{max}(n) - J_{Pareto}^{min}(n)} \qquad n = [1,2] \tag{4.18}$$

in this application, normalization is necessary in order to scale the influence of each objective function in Equation 4.17.

The second method presented in this work to decide the fittest scenario is based on an approach for optimizing the storage system operation. In this case the fittest solution will be defined as,

$$j_{Fit} = arg\min_{j}(J_{Pareto}^{Norm}(j,1) \cdot (\frac{L_{H_2}}{L_{H_2}^{max}}) + J_{Pareto}^{Norm}(j,2)) \cdot (1 - \frac{L_{H_2}}{L_{H_2}^{max}}) \tag{4.19}$$

where L_{H_2} represents the level of hydrogen stored in the storage system and $L_{H_2}^{max}$ is the maximum value allowed for the storage.

The main idea is to increase the impact of the energy curtailment objective function when storage is low, stimulating hydrogen production. On the other hand, when the storage is full, the objective function related to the transmission losses will have a higher impact, mitigating the hydrogen production and, consequently, decreasing the hydrogen stored level.

4.6 Summary

This chapter presents the case study conducted in this work and outlines the methodology used to analyze the results obtained from power grid simulations.

Primarily, the framework in which this work will be evaluated was presented, which contemplates the power grid used for the simulations and the generation and load curves that will partially determine the simulation's dynamics. Models used to represent generators and energy storage systems within the power grid are also explained.

All this information was contextualized in the optimization problem, where these models were formulated mathematically by the variables used in the OPF problem. This

chapter also presented the method used to deal with the active power curtailment in RES generators.

At last, the use of the Pareto front in order to define a set of optimal solutions considering 2 objective functions was presented, as well as two methods that can be employed in order to define the fittest within the set of solutions for each one of the scenarios analyzed.

Chapter 5

Results and discussion

In this chapter, the results obtained from the simulations of the scenarios explained in the case study will be presented. As explained earlier, the simulations are based on the implementation of a multi-objective optimization method to solve the OPF problem on a grid with the inclusion of an HSS.

The analysis will be conducted in three sections. The first section involves a comparison between the extreme cases of each objective function: minimizing the renewable energy curtailment and minimizing transmission losses in the power grid, and the multi-objective approach presented by Equation 4.17. The second section aims to investigate the impact of including an HSS in the power grid, specifically in terms of energy curtailment in RES generators, total system losses, and energy dispatched to the slack bus. Finally, the third section will present the results obtained through the implementation of the multi-objective method defined in Equation 4.19. Again the result is compared to the extreme scenarios for each objective function. It's important to note that all simulations, in this case, consider the inclusion of the HSS. For better understanding, the simulations performed in the results section are resumed in the Table 5.1

The methodology employed to evaluate each scenario is as follows: First, the optimization approach is defined, regarding the weight of each objective function. After that, the OPF problems corresponding to the four representative days will be solved consecutively. The results obtained for these four days will be examined, and then they are scaled to

represent annual operations, as explained in Figure 5.1. At last, it is verified whether the results are in agreement with the objectives and limitations determined previously.

Before presenting the annual operational results of the power grid, the Pareto frontier generated in some of the scenarios evaluated will be demonstrated.

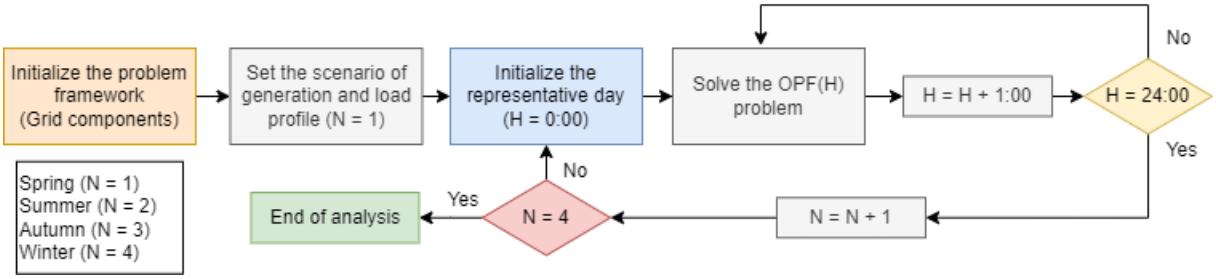

Figure 5.1: Flowchart of the procedure for conducting the annual analysis of grid operation

Table 5.1: Overview of simulation performed in each section of the Results chapter

Section	Cases analysed (optimization specification)	Legend
Multi-objective approach analysis	Minimization of transmission losses	Case 1
	Minimization of renewable energy curtailment	Case 2
	Multi-objective optimization First approach (Eq. 4.17)	Case 3
Energy storage system analysis	Minimization of transmission losses	Case 1 - no HSS
	Minimization of transmission losses with inclusion of HSS	Case 1 - HSS
	Minimization of renewable energy curtailment	Case 2 - no HSS
	Minimization of renewable energy curtailment with inclusion of HSS	Case 2 - HSS
Multi-objective approach with energy storage analysis	Minimization of transmission losses with inclusion of HSS	Case 1 - HSS
	Minimization of renewable energy curtailment with inclusion of HSS	Case 2 - HSS
	Multi-objective optimization Second approach (Eq. 4.19)	Case 3 - HSS

5.1 Pareto front

As mentioned earlier, to explore the various optimal values of solutions between the two objective functions, a Pareto front set is generated by solving the OPF problem using different weights to represent the significance of each function. In this study, the number of evaluations N was defined as 25, indicating that the resulting Pareto set will consist of 25 optimal solutions for the analyzed problem.

Figure 5.2 illustrates the Pareto frontier obtained from four different scenarios within the case study. Each simulation was conducted at 13:00 for each representative day of the year. This particular hour was selected due to its high solar production, which ensures both curtailment and flexibility to solve the case study.

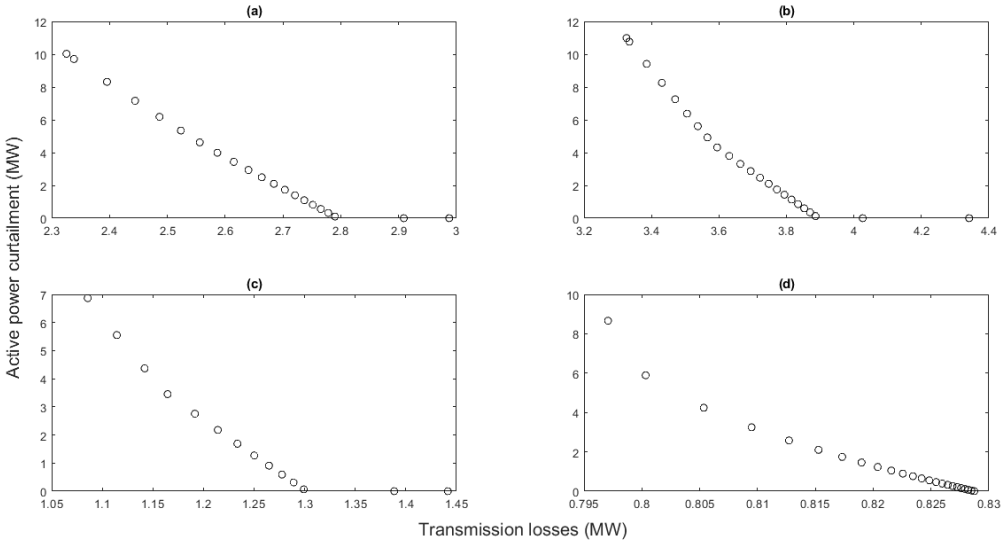

Figure 5.2: Pareto front example for each representative day, (a) Spring, (b) Summer, (c) Autumn and (d) Winter

Observing each of the illustrations, it becomes evident that the employed method effectively generated the Pareto front. Nevertheless, it is important to highlight that in some cases, as shown in charts (a), (b), and (c), some non-dominant points were also plotted. These specific points are disregarded from the normalization process and all further calculations. This exclusion is due to the fact that only dominant points can

accurately represent the optimal set that comprises the Pareto front.

5.2 Multi-objective approach analysis

The objective of this section is to compare the results of applying the multi-objective method for defining the best trade-off between both objective functions defined. Therefore, three scenarios will be evaluated,

- Case 1 - Minimize transmission losses
- Case 2 - Minimize renewable energy generation
- Case 3 - Multi-objective optimization approach

As mentioned, each representative day will be evaluated in a consecutive manner, from scenario 1 (spring) to scenario 4 (winter), in which the OPF problem will be solved on an hourly basis. This will result in a total of 96 scenarios that will represent the annual operation of the power grid. Figures 5.3 and 5.4 present the total annual active energy curtailed at each RES bus and transmission losses for each case, considering the four representative days.

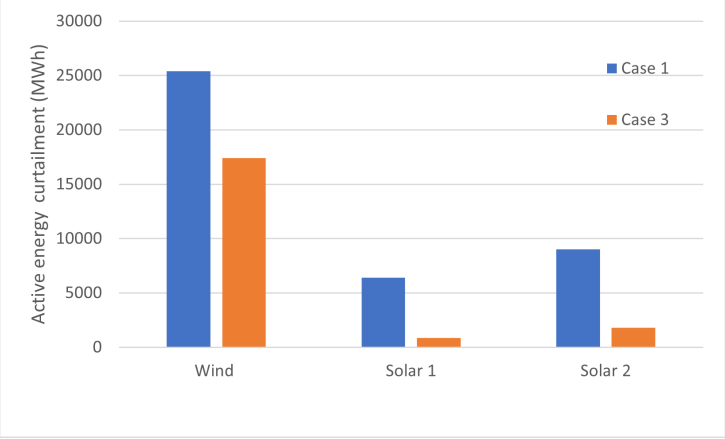

Figure 5.3: Total annual energy curtailed at each RES generator

The results obtained are as expected for each optimization approach. Case 1 exhibited the lowest transmission losses; however, it also displayed the highest energy curtailment

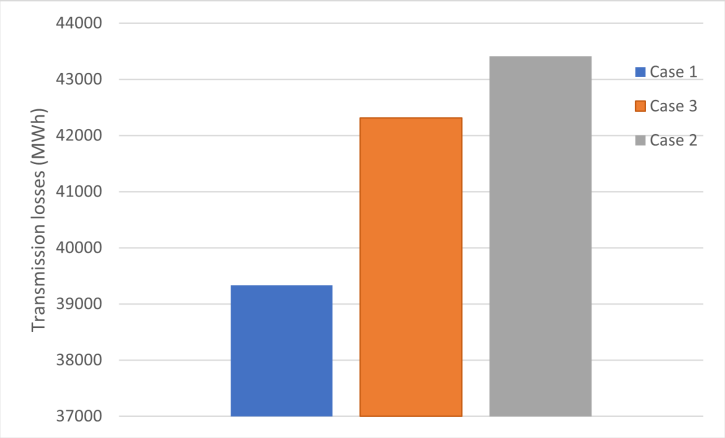

Figure 5.4: Total annual transmission loss

across all RES buses. On the other hand, case 2 produced the maximum available renewable energy, leading to the highest total transmission losses. Finally, case 3 demonstrated a trade-off between these two objective functions.

To gain a deeper understanding of the occurrences of energy curtailment and differences in the energy dispatched in the transmission line for each case, in Figures 5.5 and 5.6, these values are displayed for each OPF solved.

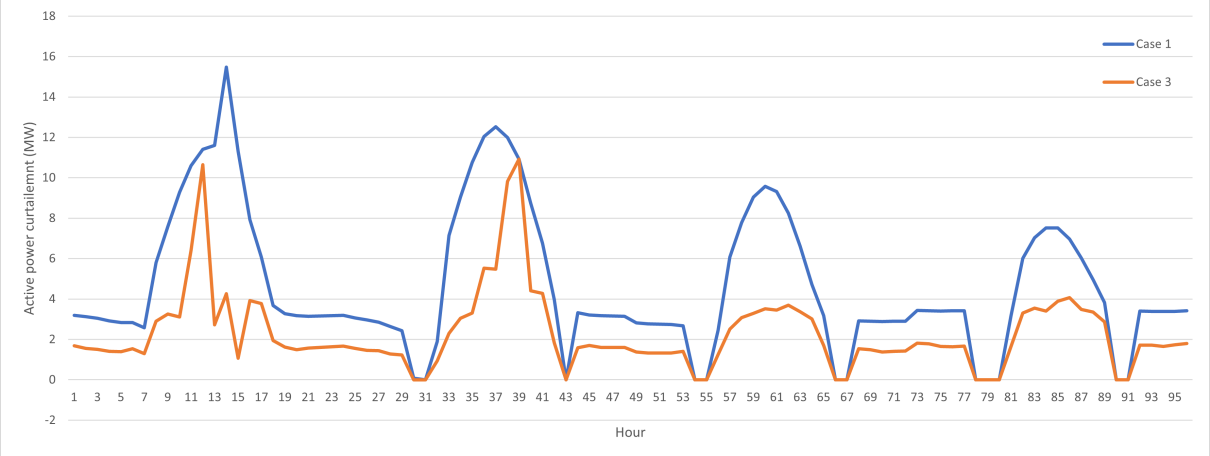

Figure 5.5: Total Active power curtailment per hour

The obtained results clearly indicate a pattern of curtailment during these four days, which occurs during the first 24 hours and repeats in a similar manner during the next days on different scales. The curtail increases drastically during the day when there is a

strong impact of solar generation, then it follows a continuous value during the moments of low load. Except in some brief moments in which the load exceeds the generation, which is more notable during the scenario representing spring and winter.

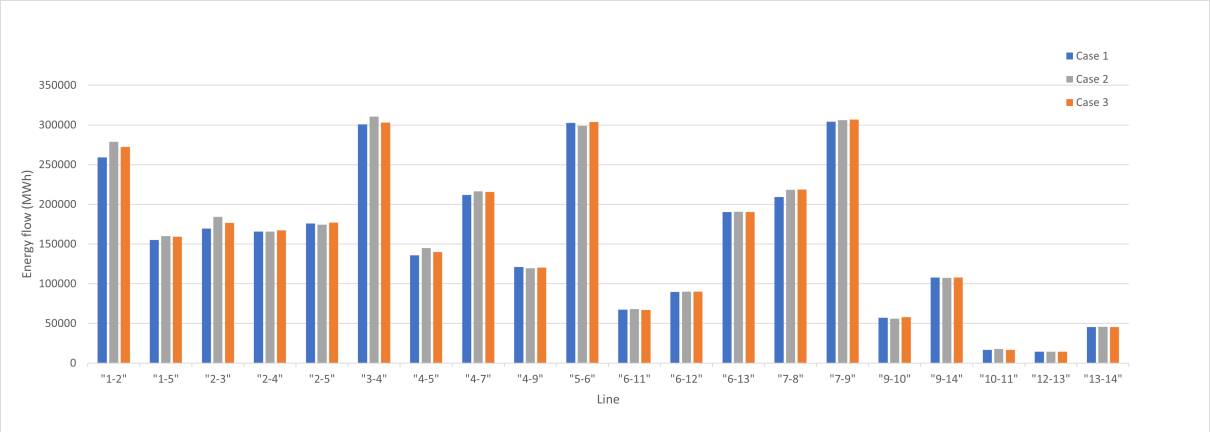

Figure 5.6: Total annual energy flow through transmission lines

A more comprehensive analysis of the power grid's annual operation is presented in Table 5.2. Some aspects worth noting are that all cases respect the constraint 5% energy generation. Furthermore, the standard deviation between these values remained below 1%.

Table 5.2: comparison of the annual operation of cases without HSS

	Case 1	Case 2	Case 3
Annual renewable energy produced (MWh)	898928	938589	919679
Annual energy loss (MWh)	39330 (4,37%)	43411 (4,62%)	42313 (4,6%)
Renewable energy curtailment (MWh)		–	
G_3	25408 (4,44%)	–	17413 (3,00%)
G_6	6384 (4,73%)	–	853 (0,62%)
G_8	9019 (4,68%)	–	1793 (0,93%)
Total renewable energy curtailed (MWh)	40812	–	20061

5.3 Energy storage system analysis

In this section, we analyze the impact of the hydrogen storage system on the overall power system's operation. Unlike the previous simulations, the comparison will be conducted

between two scenarios: one with the inclusion of the HSS and one without it. In both cases, the objective function is to minimize transmission losses. The choice of this objective function is basically because it allows energy curtailment, and therefore, is possible to verify whether the energy storage system will impact RES curtailment. Additionally, it is more practical to evaluate the simulation considering its single-objective approach.

Following a similar approach to the previous analysis, Figures 5.7 and 5.8 present a comparison of the total energy curtailment at each RES generator and the total active losses in the system. In these figures, 'Case 1' refers to the employed objective function, while 'HSS' and 'No HSS' indicate whether the hydrogen storage system was included or not.

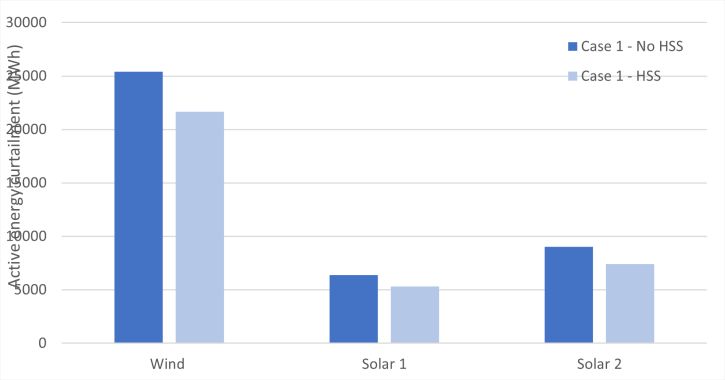

Figure 5.7: Total annual energy curtailment

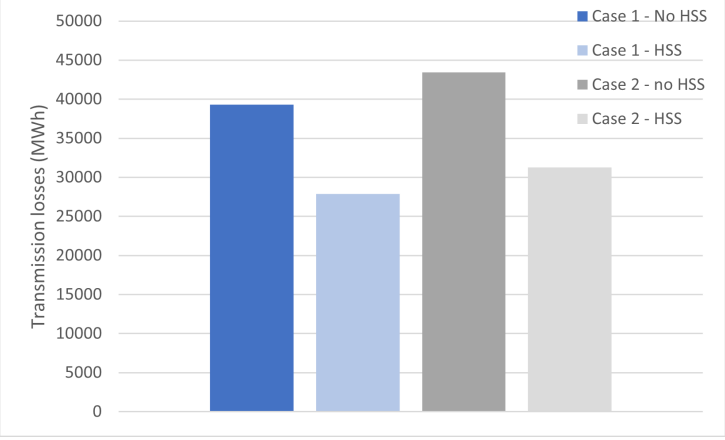

Figure 5.8: Comparing the impact of the HSS in the system active losses

The results demonstrate that both energy curtailment and transmission loss values are mitigated when the storage system is integrated into the grid. To further investigate the performance of the HSS, Figure 5.9 illustrates the levels of stored hydrogen during power grid operation. Additionally, Figure 5.10 presents a similar analysis, comparing curtailment in both cases

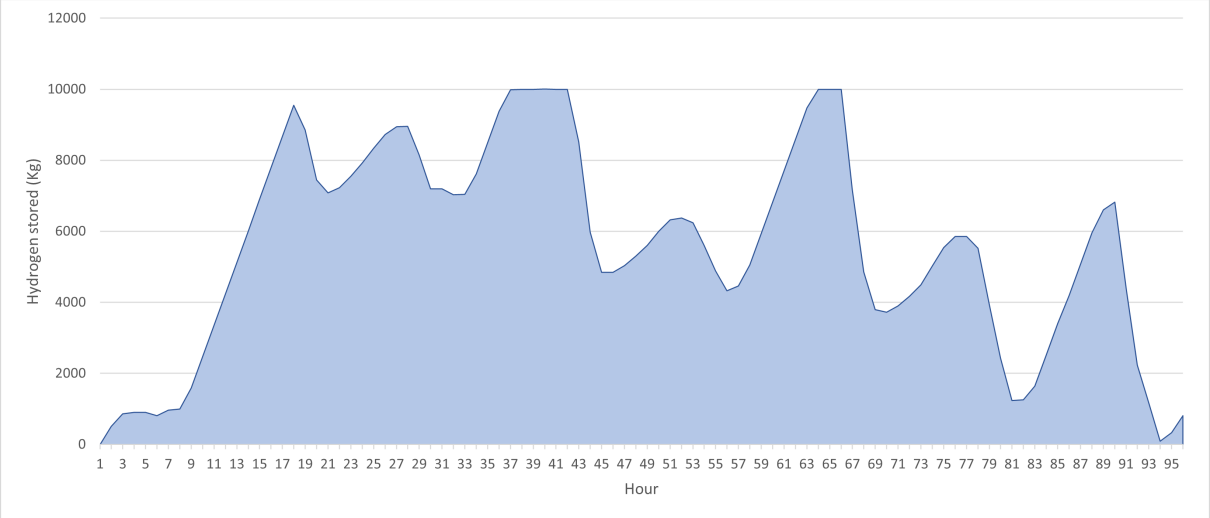

Figure 5.9: Stored hydrogen level per hour.

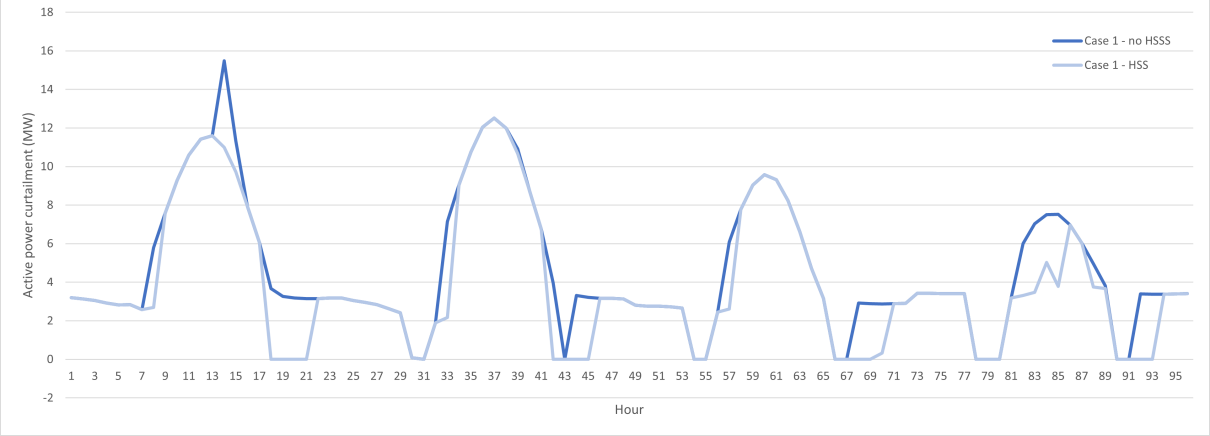

Figure 5.10: Energy curtailment per hour

The curve associated with the hydrogen storage level exhibits a pattern. There is an increase in stored energy during periods of high generation, as expected, and it is also evident that the HSS supplies energy to the system during moments when generation

is insufficient. At certain moments, the storage system reaches its maximum capacity of 10000 kg; however, not for long periods of time, which reinforces the decision regarding the size defined for the storage. Regarding the energy curtailment curve, there is a reduction in the amount of energy curtailment. Even though, the dynamics in both cases remain quite similar.

Additional evidence supporting the impact of HSS on total power grid losses is presented in Figure 5.11, which shows the total energy flow in each transmission line. In particular, lines located close to bar 3, where the HSS is installed, exhibit a significant reduction in power flow. Furthermore, the power dispatched to the slack bar presents the greatest impact, with its power dispatched reduced by 33%. The value can be verified in Figure 5.12, which compares the power traded by the slack bar in both scenarios.

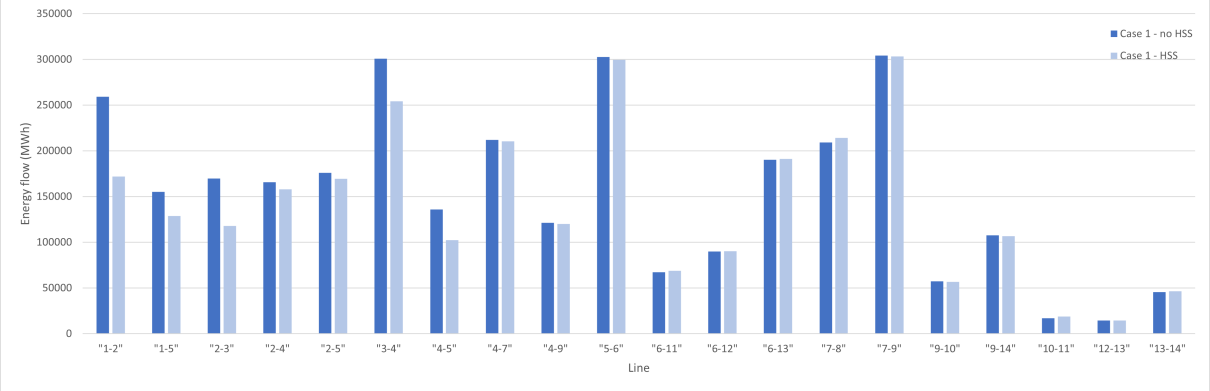

Figure 5.11: Total annual energy flow through the transmission lines during the representative days

5.4 Multi-objective approach with energy storage analysis

At last, in this section, it is analyzed the application of the multi-objective approach in the scenario with the HSS. As explained earlier, the Pareto front offers a vast number of options for optimizing the problem, then it is necessary to define the fittest among them.

This section presents the results of the method introduced in Equation 4.14, where the

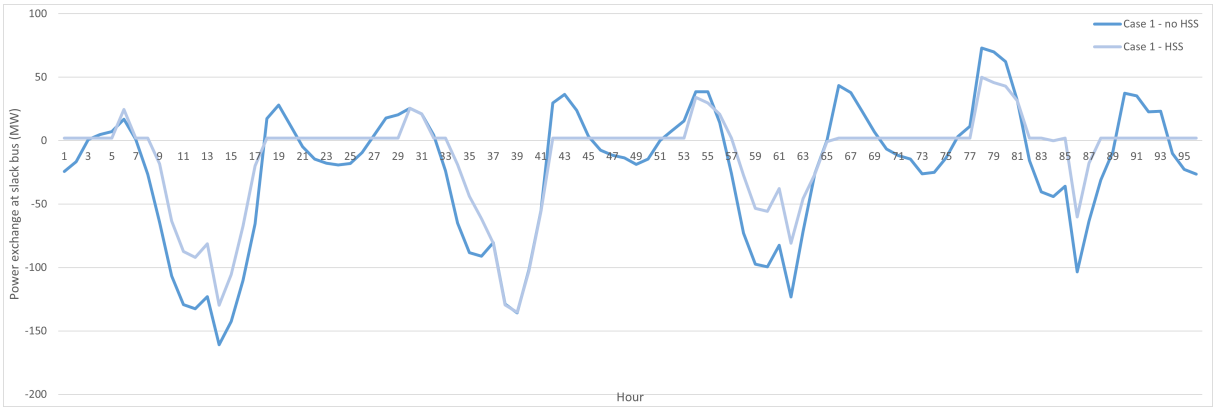

Figure 5.12: Power exchange with slack bus per hour

level of hydrogen stored in the HSS serves as a decision variable to determine the most fitting solution among all the optimal points in the Pareto set. Figures 5.13 and 5.14 offer a comparison regarding active energy curtailed and transmission losses, with respect to the extreme cases of the objective functions with the multi-objective method employed. As previously: Case 1 represents the minimization of transmission losses, Case 2 focuses on maximizing RES generation, and Case 3 employs the multi-objective approach to the problem.

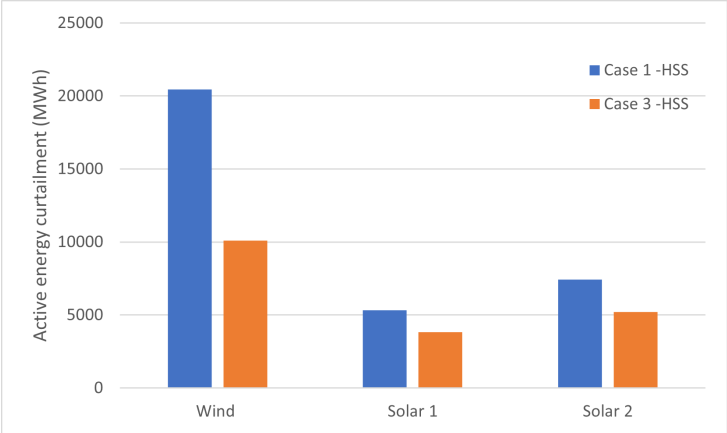

Figure 5.13: Total annual energy curtailment in RES generators

The results demonstrate an improvement in terms of energy curtailment, showing a reduction of 43% when compared to Case 1. Furthermore, the increase in transmission losses remains almost unchanged, with an increase of 3% regarding the values presented

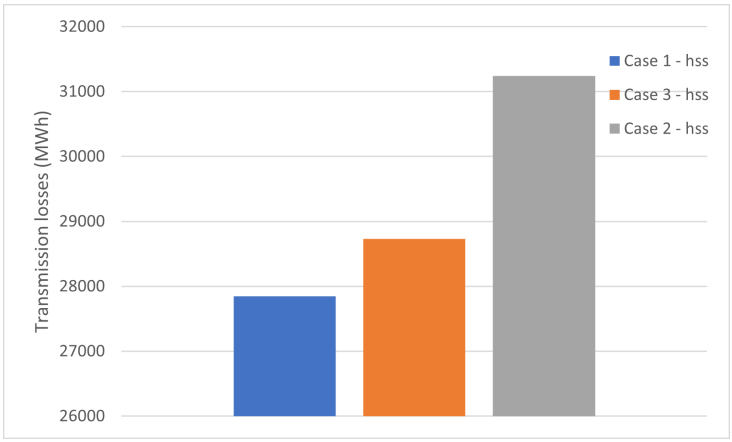

Figure 5.14: Total annual transmission losses

in Case 1.

Figure 5.15 shows the distinctions in the energy curtailment profiles between the previously presented cases. Case 3 is omitted from this chart, as the energy curtailment is non-existent.

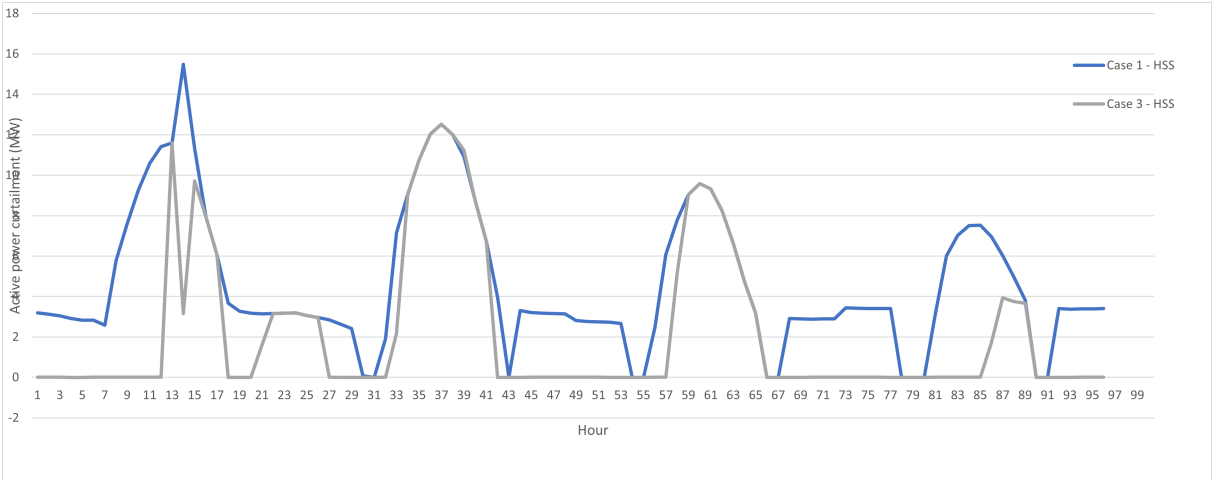

Figure 5.15: Total annual energy curtailment per hour

Table 5.3 presents the annual results for each case discussed in this section. All the values support the observations that have been discussed so far. In terms of the curtailment constraints, all cases respected the 5% limitation, and the standard deviation among the curtailment values also remained below 1%.

Table 5.3: Comparison of the annual operation of cases with HSS

	Case 1	Case 2	Case 3
Annual renewable energy produced (MWh)	906559	938589	920618
Annual energy loss (MWh)	27846 (3,07%)	31242 (3,32%)	28727 (3,12%)
Renewable energy curtailment (MWh)	20437 (3,54%)	–	10087 (1,72%)
G3	5323 (3,91%)	–	3828 (2,79%)
G6	7419 (3,81%)	–	5205 (2,64%)
G8		–	
Total renewable energy curtailed (MWh)	33180	–	19121

5.5 Summary

This chapter presents the results obtained in this work. Initially, the section introduces an explanation of the methodology used for simulating the annual grid operation and outlines the structure of the chapter, which includes a figure and a table to aid the reader's understanding.

The following sections are organized according to the objectives expected from the simulations. First, an analysis of multi-objective optimization compared to the single-objective approach is conducted. The results obtained demonstrate a trade-off between the objective functions, highlighting the effectiveness of the multi-objective approach.

The next section examines the impact of the HSS on the grid transmission losses and the curtailment of renewable energy. As expected, the inclusion of a storage system improves the overall operation concerning these factors.

Finally, the results of the simulations considering a multi-objective approach designed for operation with the storage system are presented. The data obtained indicate an improvement in operation, with a reduction in the curtailment of all RES generators, and even so, the transmission losses were not significantly affected.

Chapter 6

Conclusion and Future Work

This study presents an analysis of the application of a multi-objective optimization approach for optimizing energy dispatch in renewable sources-based generators. Additionally, the study introduces a hydrogen storage system in the power grid and evaluates its impact on renewable energy curtailment and transmission losses. The framework of this study uses the IEEE 14-bus electric network as the foundational scenario and four representative days were selected to simulate a year of grid operation, with load and generation profiles designed from real data collected from available data sets. All optimization problems were solved using a MATLAB tool named MATPOWER, and the employed multi-objective algorithm was the goal attainment approach.

The initial analysis were conducted without the inclusion of the HSS in the power grid. This approach aimed to analyze the implementation of the multi-objective approach differently from the standard single-objective optimization considering two objective functions. The results primarily demonstrated the success of the multi-objective approach in generating a trade-off between the studied objective functions and generating a set of optimal solutions that could be employed in different methods to optimize the dispatch of RES energy.

The subsequent analysis aimed to investigate the impact of the hydrogen storage system on the power grid. The expectation was that the system could reduce the active power

curtailment in RES generators and serve as a decision variable for the multi-objective optimization approach. The outcomes revealed that the HSS improved the overall operation. It not only mitigated curtailment across all RES generators but also reduced total transmission losses. The results indicate a decrease in the energy traded between the grid and the slack bus, suggesting also an improvement regarding grid autonomy.

In the last analysis, a second approach for the multi-objective case was presented. In this new scenario, the hydrogen storage level served as a decision variable to define the optimal solution on the Pareto front. This case involved comparing both extreme cases of the objective function, including the presence of the HSS. The results demonstrated that the multi-objective approach had operational improvements compared to the other methods. In a comparison with the extreme case of minimal energy losses, there was mitigation of the RES curtailment, however, the transmission losses were not significantly impacted.

Ultimately, the primary objective of the study was achieved. Two approaches were presented to apply multi-objective optimization algorithms to solve the optimal power flow problem, and the results proved to be satisfactory. Regarding energy curtailment, the study also confirmed that all cases under investigation respect the annual curtailment limits, with a standard deviation between these values below 1%.

In terms of future improvements, the author suggests:

- Economic analysis of the problem
- Implementation of a multi-period OPF
- Optimization of the hydrogen storage system's placement and device size.
- Comparison between different storage methods.

References

[1] L. Bird, D. Lew, M. Milligan, *et al.*, "Wind and solar energy curtailment: A review of international experience," *Renewable and Sustainable Energy Reviews*, vol. 65, pp. 577–586, 2016, ISSN: 1364-0321. DOI: https://doi.org/10.1016/j.rser.2016.06.082. [Online]. Available: https://www.sciencedirect.com/science/article/pii/S1364032116303161.

[2] REN21, *Renewables 2023: Global status report*, 2023. [Online]. Available: https://www.ren21.net/.

[3] P. Sinha, K. Paul, S. Deb, and S. Sachan, "Comprehensive review based on the impact of integrating electric vehicle and renewable energy sources to the grid," *Energies*, vol. 16, no. 6, 2023, ISSN: 1996-1073. DOI: 10.3390/en16062924. [Online]. Available: https://www.mdpi.com/1996-1073/16/6/2924.

[4] L. Bird, D. Lew, M. Milligan, *et al.*, "Wind and solar energy curtailment: A review of international experience," *Renewable and Sustainable Energy Reviews*, vol. 65, pp. 577–586, 2016, ISSN: 1364-0321. DOI: https://doi.org/10.1016/j.rser.2016.06.082. [Online]. Available: https://www.sciencedirect.com/science/article/pii/S1364032116303161.

[5] European Parliament, Council of the European Union, *Regulation (eu) 2019/943 of the european parliament and of the council of 5 june 2019 on the internal market for electricity*, 2019. [Online]. Available: https://www.ren21.net/.

[6] F. Meier, C. Töbermann, and M. Braun, "Retrospective optimal power flow for low discriminating active power curtailment," in *2019 IEEE Milan PowerTech*, 2019, pp. 1–6. DOI: 10.1109/PTC.2019.8810818.

[7] P. Wiest, K. Rudion, and A. Probst, "Optimization of power feed-in curtailment from res and its consideration within grid planning," in *2017 IEEE Manchester PowerTech*, 2017, pp. 1–6. DOI: 10.1109/PTC.2017.7980801.

[8] J. Yap and B. McLellan, "A historical analysis of hydrogen economy research, development, and expectations, 1972 to 2020," *Environments*, vol. 10, no. 1, p. 11, Jan. 2023. DOI: 10.3390/environments10010011. [Online]. Available: https://doi.org/10.3390/environments10010011.

[9] European commission, *European clean hydrogen alliance roadmap on standardisation*, 2023. [Online]. Available: https://ec.europa.eu/docsroom/documents/53721.

[10] O. Ehret and K. Bonhoff, "Hydrogen as a fuel and energy storage: Success factors for the german energiewende," *International Journal of Hydrogen Energy*, vol. 40, no. 15, pp. 5526–5533, 2015, ISSN: 0360-3199. DOI: https://doi.org/10.1016/j.ijhydene.2015.01.176. [Online]. Available: https://www.sciencedirect.com/science/article/pii/S036031991500275X.

[11] R. Moliner, M. Lázaro, and I. Suelves, "Analysis of the strategies for bridging the gap towards the hydrogen economy," *International Journal of Hydrogen Energy*, vol. 41, no. 43, pp. 19 500–19 508, 2016, The 5th Iberian Symposium on Hydrogen, Fuel Cells and Advanced Batteries (HYCELTEC 2015), 5-8 July 2015, Tenerife, Spain, ISSN: 0360-3199. DOI: https://doi.org/10.1016/j.ijhydene.2016.06.202. [Online]. Available: https://www.sciencedirect.com/science/article/pii/S0360319916303287.

[12] J. O. Bockris, "The hydrogen economy: Its history," *International Journal of Hydrogen Energy*, vol. 38, no. 6, pp. 2579–2588, 2013, ISSN: 0360-3199. DOI: https:

//doi.org/10.1016/j.ijhydene.2012.12.026. [Online]. Available: https://www.sciencedirect.com/science/article/pii/S036031991202664X.

[13] European commission, *Towards a european hydrogen energy roadmap*, 2023. [Online]. Available: https://trimis.ec.europa.eu/project/towards-european-hydrogen-energy-roadmap.

[14] European commission, *Hydrogen energy and fuel cells. a vision of our future*, 2003. [Online]. Available: https://inis.iaea.org/search/search.aspx?orig_q=RN%3A37121708.

[15] F. Dawood, M. Anda, and G. Shafiullah, "Hydrogen production for energy: An overview," *International Journal of Hydrogen Energy*, vol. 45, no. 7, pp. 3847–3869, 2020, ISSN: 0360-3199. DOI: https://doi.org/10.1016/j.ijhydene.2019.12.059. [Online]. Available: https://www.sciencedirect.com/science/article/pii/S0360319919345926.

[16] A. Ajanovic, M. Sayer, and R. Haas, "The economics and the environmental benignity of different colors of hydrogen," *International Journal of Hydrogen Energy*, vol. 47, no. 57, pp. 24 136–24 154, 2022, Hydrogen Society, ISSN: 0360-3199. DOI: https://doi.org/10.1016/j.ijhydene.2022.02.094. [Online]. Available: https://www.sciencedirect.com/science/article/pii/S0360319922007066.

[17] IEA, *Global hydrogen review 2022 – analysis*. [Online]. Available: https://www.iea.org/reports/global-hydrogen-review-2022.

[18] A. M. Abdalla, S. Hossain, O. B. Nisfindy, A. T. Azad, M. Dawood, and A. K. Azad, "Hydrogen production, storage, transportation and key challenges with applications: A review," *Energy Conversion and Management*, vol. 165, pp. 602–627, Jun. 2018. DOI: 10.1016/j.enconman.2018.03.088. [Online]. Available: https://doi.org/10.1016/j.enconman.2018.03.088.

[19] IEA, *Hydrogen production and storage*. [Online]. Available: https://www.iea.org/reports/hydrogen-production-and-storage.

[20] Y. M. Welaya, M. M. E. Gohary, and N. R. Ammar, "Steam and partial oxidation reforming options for hydrogen production from fossil fuels for PEM fuel cells," *Alexandria Engineering Journal*, vol. 51, no. 2, pp. 69–75, Jun. 2012. DOI: 10.1016/j.aej.2012.03.001. [Online]. Available: https://doi.org/10.1016/j.aej.2012.03.001.

[21] S. Grigoriev, V. Fateev, D. Bessarabov, and P. Millet, "Current status, research trends, and challenges in water electrolysis science and technology," *International Journal of Hydrogen Energy*, vol. 45, no. 49, pp. 26 036–26 058, Oct. 2020. DOI: 10.1016/j.ijhydene.2020.03.109. [Online]. Available: https://doi.org/10.1016/j.ijhydene.2020.03.109.

[22] K. Zeng and D. Zhang, "Recent progress in alkaline water electrolysis for hydrogen production and applications," *Progress in Energy and Combustion Science*, vol. 36, no. 3, pp. 307–326, 2010, ISSN: 0360-1285. DOI: https://doi.org/10.1016/j.pecs.2009.11.002. [Online]. Available: https://www.sciencedirect.com/science/article/pii/S0360128509000598.

[23] S. S. Kumar and V. Himabindu, "Hydrogen production by PEM water electrolysis – a review," *Materials Science for Energy Technologies*, vol. 2, no. 3, pp. 442–454, Dec. 2019. DOI: 10.1016/j.mset.2019.03.002. [Online]. Available: https://doi.org/10.1016/j.mset.2019.03.002.

[24] J. Chi and H. Yu, "Water electrolysis based on renewable energy for hydrogen production," *Chinese Journal of Catalysis*, vol. 39, no. 3, pp. 390–394, Mar. 2018. DOI: 10.1016/s1872-2067(17)62949-8. [Online]. Available: https://doi.org/10.1016/s1872-2067(17)62949-8.

[25] F. M. Sapountzi, J. M. Gracia, C. (.-J. Weststrate, H. O. Fredriksson, and J. (Niemantsverdriet, "Electrocatalysts for the generation of hydrogen, oxygen and synthesis gas," *Progress in Energy and Combustion Science*, vol. 58, pp. 1–35, Jan. 2017. DOI: 10.1016/j.pecs.2016.09.001. [Online]. Available: https://doi.org/10.1016/j.pecs.2016.09.001.

[26] R. Hren, A. Vujanović, Y. V. Fan, J. J. Klemeš, D. Krajnc, and L. Čuček, "Hydrogen production, storage and transport for renewable energy and chemicals: An environmental footprint assessment," *Renewable and Sustainable Energy Reviews*, vol. 173, p. 113 113, Mar. 2023. DOI: 10.1016/j.rser.2022.113113. [Online]. Available: https://doi.org/10.1016/j.rser.2022.113113.

[27] M. Yang, R. Hunger, S. Berrettoni, B. Sprecher, and B. Wang, "A review of hydrogen storage and transport technologies," *Clean Energy*, vol. 7, no. 1, pp. 190–216, Feb. 2023. DOI: 10.1093/ce/zkad021. [Online]. Available: https://doi.org/10.1093/ce/zkad021.

[28] W. Colella, S. W. Cha, R. P. O'Hayre, and F. B. Prinz, "Fuel cell fundamentals," in John Wiley Sons, Ltd, 2016, ch. 1, pp. 1–24, ISBN: 9781119191766. DOI: https://doi.org/10.1002/9781119191766.ch1. [Online]. Available: https://onlinelibrary.wiley.com/doi/abs/10.1002/9781119191766.ch1.

[29] O. Z. Sharaf and M. F. Orhan, "An overview of fuel cell technology: Fundamentals and applications," *Renewable and Sustainable Energy Reviews*, vol. 32, pp. 810–853, Apr. 2014. DOI: 10.1016/j.rser.2014.01.012. [Online]. Available: https://doi.org/10.1016/j.rser.2014.01.012.

[30] R. Guo, Q. Li, and N. Zhao, "An overview of grid-connected fuel cell system for grid support," *Energy Reports*, vol. 8, pp. 884–892, Nov. 2022. DOI: 10.1016/j.egyr.2022.05.211. [Online]. Available: https://doi.org/10.1016/j.egyr.2022.05.211.

[31] M. Ban, J. Yu, M. Shahidehpour, and Y. Yao, "Integration of power-to-hydrogen in day-ahead security-constrained unit commitment with high wind penetration," *Journal of Modern Power Systems and Clean Energy*, vol. 5, no. 3, pp. 337–349, 2017. DOI: 10.1007/s40565-017-0277-0.

[32] M. Yue, H. Lambert, E. Pahon, R. Roche, S. Jemei, and D. Hissel, "Hydrogen energy systems: A critical review of technologies, applications, trends and challenges," *Renewable and Sustainable Energy Reviews*, vol. 146, p. 111 180, Aug. 2021. DOI:

10.1016/j.rser.2021.111180. [Online]. Available: https://doi.org/10.1016/j.rser.2021.111180.

[33] J. Carpentier, "Optimal power flows," *International Journal of Electrical Power Energy Systems*, vol. 1, no. 1, pp. 3–15, 1979, ISSN: 0142-0615. DOI: https://doi.org/10.1016/0142-0615(79)90026-7. [Online]. Available: https://www.sciencedirect.com/science/article/pii/0142061579900267.

[34] J. Zhu, *Optimization of Power System Operation*. New Jersey: John Wiley Son, 2009.

[35] S. Frank, I. Steponavice, and S. Rebennack, "Optimal power flow: A bibliographic survey i," *Energy Systems*, vol. 3, no. 3, pp. 221–258, Apr. 2012. DOI: 10.1007/s12667-012-0056-y. [Online]. Available: https://doi.org/10.1007/s12667-012-0056-y.

[36] H. Mataifa, S. Krishnamurthy, and C. Kriger, "An efficient primal-dual interior-point algorithm for volt/var optimization in rectangular voltage coordinates," *IEEE Access*, vol. 11, pp. 36 890–36 906, 2023. DOI: 10.1109/ACCESS.2023.3266421.

[37] S. Frank, I. Steponavičė, and S. Rebennack, "Optimal power flow: A bibliographic survey ii," *Energy Systems*, vol. 3, Sep. 2012. DOI: 10.1007/s12667-012-0057-x.

[38] M. J. Kochenderfer and T. A. Wheeler, *Algorithms for Optimization*. The MIT Press, 2019, ISBN: 0262039427.

[39] J. D. Glover and Sarma, *Power Systems Analysis and Design*. USA: PWS Publishing Co., 1987, ISBN: 0534078605.

[40] N. Karmarkar, "A new polynomial-time algorithm for linear programming," *Combinatorica*, vol. 4, no. 4, pp. 373–395, Dec. 1984. DOI: 10.1007/bf02579150. [Online]. Available: https://doi.org/10.1007/bf02579150.

[41] J. Nocedal and S. J. Wright, *Numerical Optimization*, 2e. New York, NY, USA: Springer, 2006.

[42] A. Pedroso, Y. Amoura, A. I. Pereira, and Â. Ferreira, "A hybrid genetic algorithm for optimal active power curtailment considering renewable energy generation," in *Computational Science and Its Applications – ICCSA 2023 Workshops*, O. Gervasi, B. Murgante, A. M. A. C. Rocha, *et al.*, Eds., Cham: Springer Nature Switzerland, 2023, pp. 479–494, ISBN: 978-3-031-37108-0.

[43] J. C. Das, *Load Flow Optimization and Optimal Power Flow*. CRC Press, Oct. 2017. DOI: 10.1201/9781351228299. [Online]. Available: https://doi.org/10.1201/9781351228299.

[44] R. Marler and J. Arora, "Survey of multi-objective optimization methods for engineering," *Structural and Multidisciplinary Optimization*, vol. 26, no. 6, pp. 369–395, Apr. 2004. DOI: 10.1007/s00158-003-0368-6. [Online]. Available: https://doi.org/10.1007/s00158-003-0368-6.

[45] K. Deb, A. Pratap, S. Agarwal, and T. Meyarivan, "A fast and elitist multiobjective genetic algorithm: Nsga-ii," *IEEE Transactions on Evolutionary Computation*, vol. 6, no. 2, pp. 182–197, 2002. DOI: 10.1109/4235.996017.

[46] F. Gembicki and Y. Haimes, "Approach to performance and sensitivity multiobjective optimization: The goal attainment method," *IEEE Transactions on Automatic Control*, vol. 20, no. 6, pp. 769–771, 1975. DOI: 10.1109/TAC.1975.1101105.

[47] J. G. Lin, "On min-norm and min-max methods of multi-objective optimization," *Mathematical Programming*, vol. 103, no. 1, pp. 1–33, Sep. 2003. DOI: 10.1007/s10107-003-0462-y. [Online]. Available: https://doi.org/10.1007/s10107-003-0462-y.

[48] S. Rahmani and N. Amjady, "Enhanced goal attainment method for solving multi-objective security-constrained optimal power flow considering dynamic thermal rating of lines," *Applied Soft Computing*, vol. 77, pp. 41–49, 2019, ISSN: 1568-4946. DOI: https://doi.org/10.1016/j.asoc.2019.01.014. [Online]. Available: https://www.sciencedirect.com/science/article/pii/S1568494619300183.

[49] Illinois Center for a Smarter Electric Grid, *IEEE 14-Bus System*, https://icseg.iti.illinois.edu/ieee-14-bus-system/, [Accessed 22-08-2023].

[50] F. Angizeh, *Dataset on hourly load profiles for a set of 24 facilities from industrial, commercial, and residential end-use sectors*, 2020. DOI: 10.17632/RFNP2D3KJP.1. [Online]. Available: https://data.mendeley.com/datasets/rfnp2d3kjp/1.

[51] H. Yang, L. Lu, and W. Zhou, "A novel optimization sizing model for hybrid solar-wind power generation system," *Solar Energy*, vol. 81, no. 1, pp. 76–84, 2007, ISSN: 0038-092X. DOI: https://doi.org/10.1016/j.solener.2006.06.010. [Online]. Available: https://www.sciencedirect.com/science/article/pii/S0038092X06001836.

[52] Vestas, *V100-2.0 mw*, [Accessed 20-08-2023]. [Online]. Available: https://www.vestas.com/en/products/2-mw-platform/V100-2-0-MW.

[53] Open-meteo, *Free weather API*. [Online]. Available: https://open-meteo.com/.

[54] Y. M. Atwa, E. F. El-Saadany, M. M. A. Salama, and R. Seethapathy, "Optimal renewable resources mix for distribution system energy loss minimization," *IEEE Transactions on Power Systems*, vol. 25, no. 1, pp. 360–370, 2010. DOI: 10.1109/TPWRS.2009.2030276.

[55] Z. Meng, Q. He, X. Shi, D. Cao, and D. Du, "Research on energy utilization of wind-hydrogen coupled energy storage power generation system," *Separation and Purification Technology*, vol. 313, p. 123 439, 2023. DOI: https://doi.org/10.1016/j.seppur.2023.123439. [Online]. Available: https://www.sciencedirect.com/science/article/pii/S1383586623003477.

[56] Nel hydrogen, *Nel Hydrogen | Unlocking the potential of renewables.* https://nelhydrogen.com/, [Accessed 20-08-2023].

[57] Ballard, *Fuel cell power products fuel cell solutions.* https://www.ballard.com/fuel-cell-solutions/fuel-cell-power-products, [Accessed 20-08-2023].